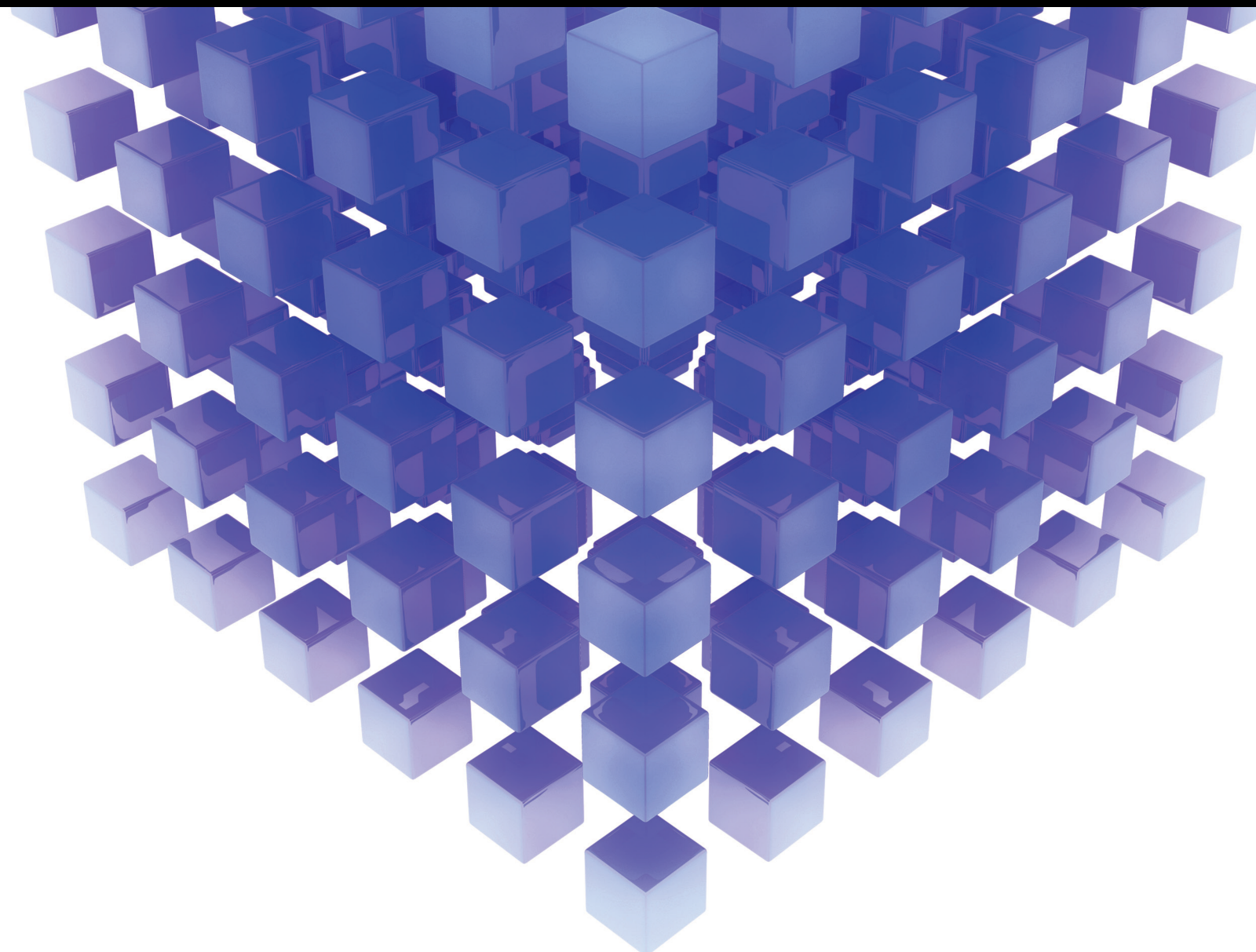


Advanced Computational Methods for Inverse Problems in Structural Engineering

Lead Guest Editor: Chen Yang

Guest Editors: Baijie Qiao, Hailing Fu, Lei Wang, Lingling Lu, and Menghui Xu





Advanced Computational Methods for Inverse Problems in Structural Engineering

Mathematical Problems in Engineering

Advanced Computational Methods for Inverse Problems in Structural Engineering

Lead Guest Editor: Chen Yang


Guest Editors: Baijie Qiao, Hailing Fu, Lei Wang,
Lingling Lu, and Menghui Xu



Copyright © 2022 Hindawi Limited. All rights reserved.

This is a special issue published in “Mathematical Problems in Engineering.” All articles are open access articles distributed under the Creative Commons Attribution License, which permits unrestricted use, distribution, and reproduction in any medium, provided the original work is properly cited.

Chief Editor

Guangming Xie , China

Academic Editors

Kumaravel A , India
Waqas Abbasi, Pakistan
Mohamed Abd El Aziz , Egypt
Mahmoud Abdel-Aty , Egypt
Mohammed S. Abdo, Yemen
Mohammad Yaghoub Abdollahzadeh
Jamalabadi , Republic of Korea
Rahib Abiyev , Turkey
Leonardo Acho , Spain
Daniela Addessi , Italy
Arooj Adeel , Pakistan
Waleed Adel , Egypt
Ramesh Agarwal , USA
Francesco Aggogeri , Italy
Ricardo Aguilar-Lopez , Mexico
Afaq Ahmad , Pakistan
Naveed Ahmed , Pakistan
Elias Aifantis , USA
Akif Akgul , Turkey
Tareq Al-shami , Yemen
Guido Ala, Italy
Andrea Alaimo , Italy
Reza Alam, USA
Osamah Albahri , Malaysia
Nicholas Alexander , United Kingdom
Salvatore Alfonzetti, Italy
Ghous Ali , Pakistan
Nouman Ali , Pakistan
Mohammad D. Aliyu , Canada
Juan A. Almendral , Spain
A.K. Alomari, Jordan
José Domingo Álvarez , Spain
Cláudio Alves , Portugal
Juan P. Amezcua-Sanchez, Mexico
Mukherjee Amitava, India
Lionel Amodeo, France
Sebastian Anita, Romania
Costanza Arico , Italy
Sabri Arik, Turkey
Fausto Arpino , Italy
Rashad Asharabi , Saudi Arabia
Farhad Aslani , Australia
Mohsen Asle Zaeem , USA

Andrea Avanzini , Italy
Richard I. Avery , USA
Viktor Avrutin , Germany
Mohammed A. Awadallah , Malaysia
Francesco Aymerich , Italy
Sajad Azizi , Belgium
Michele Baccocchi , Italy
Seungik Baek , USA
Khaled Bahlali, France
M.V.A Raju Bahubalendruni, India
Pedro Balaguer , Spain
P. Balasubramaniam, India
Stefan Balint , Romania
Ines Tejado Balsera , Spain
Alfonso Banos , Spain
Jerzy Baranowski , Poland
Tudor Barbu , Romania
Andrzej Bartoszewicz , Poland
Sergio Baselga , Spain
S. Caglar Baslamisli , Turkey
David Bassir , France
Chiara Bedon , Italy
Azeddine Beghdadi, France
Andriette Bekker , South Africa
Francisco Beltran-Carbajal , Mexico
Abdellatif Ben Makhlof , Saudi Arabia
Denis Benasciutti , Italy
Ivano Benedetti , Italy
Rosa M. Benito , Spain
Elena Benvenuti , Italy
Giovanni Berselli, Italy
Michele Betti , Italy
Pietro Bia , Italy
Carlo Bianca , France
Simone Bianco , Italy
Vincenzo Bianco, Italy
Vittorio Bianco, Italy
David Bigaud , France
Sardar Muhammad Bilal , Pakistan
Antonio Bilotta , Italy
Sylvio R. Bistafa, Brazil
Chiara Boccaletti , Italy
Rodolfo Bontempo , Italy
Alberto Borboni , Italy
Marco Bortolini, Italy

Paolo Boscariol, Italy
Daniela Boso , Italy
Guillermo Botella-Juan, Spain
Abdesselem Boulkroune , Algeria
Boulaïd Boulkroune, Belgium
Fabio Bovenga , Italy
Francesco Braghin , Italy
Ricardo Branco, Portugal
Julien Bruchon , France
Matteo Bruggi , Italy
Michele Brun , Italy
Maria Elena Bruni, Italy
Maria Angela Butturi , Italy
Bartłomiej Błachowski , Poland
Dhanamjayulu C , India
Raquel Caballero-Águila , Spain
Filippo Cacace , Italy
Salvatore Caddemi , Italy
Zuowei Cai , China
Roberto Caldelli , Italy
Francesco Cannizzaro , Italy
Maosen Cao , China
Ana Carpio, Spain
Rodrigo Carvajal , Chile
Caterina Casavola, Italy
Sara Casciati, Italy
Federica Caselli , Italy
Carmen Castillo , Spain
Inmaculada T. Castro , Spain
Miguel Castro , Portugal
Giuseppe Catalanotti , United Kingdom
Alberto Cavallo , Italy
Gabriele Cazzulani , Italy
Fatih Vehbi Celebi, Turkey
Miguel Cerrolaza , Venezuela
Gregory Chagnon , France
Ching-Ter Chang , Taiwan
Kuei-Lun Chang , Taiwan
Qing Chang , USA
Xiaoheng Chang , China
Prasenjit Chatterjee , Lithuania
Kacem Chehdi, France
Peter N. Cheimets, USA
Chih-Chiang Chen , Taiwan
He Chen , China

Kebing Chen , China
Mengxin Chen , China
Shyi-Ming Chen , Taiwan
Xizhong Chen , Ireland
Xue-Bo Chen , China
Zhiwen Chen , China
Qiang Cheng, USA
Zeyang Cheng, China
Luca Chiapponi , Italy
Francisco Chicano , Spain
Tirivanhu Chinyoka , South Africa
Adrian Chmielewski , Poland
Seongim Choi , USA
Gautam Choubey , India
Hung-Yuan Chung , Taiwan
Yusheng Ci, China
Simone Cinquemani , Italy
Roberto G. Citarella , Italy
Joaquim Ciurana , Spain
John D. Clayton , USA
Piero Colajanni , Italy
Giuseppina Colicchio, Italy
Vassilios Constantoudis , Greece
Enrico Conte, Italy
Alessandro Contento , USA
Mario Cools , Belgium
Gino Cortellessa, Italy
Carlo Cosentino , Italy
Paolo Crippa , Italy
Erik Cuevas , Mexico
Guozeng Cui , China
Mehmet Cunkas , Turkey
Giuseppe D'Aniello , Italy
Peter Dabnichki, Australia
Weizhong Dai , USA
Zhifeng Dai , China
Purushothaman Damodaran , USA
Sergey Dashkovskiy, Germany
Adiel T. De Almeida-Filho , Brazil
Fabio De Angelis , Italy
Samuele De Bartolo , Italy
Stefano De Miranda , Italy
Filippo De Monte , Italy

José António Fonseca De Oliveira
Correia , Portugal
Jose Renato De Sousa , Brazil
Michael Defoort, France
Alessandro Della Corte, Italy
Laurent Dewasme , Belgium
Sanku Dey , India
Gianpaolo Di Bona , Italy
Roberta Di Pace , Italy
Francesca Di Puccio , Italy
Ramón I. Diego , Spain
Yannis Dimakopoulos , Greece
Hasan Dinçer , Turkey
José M. Domínguez , Spain
Georgios Dounias, Greece
Bo Du , China
Emil Dumić, Croatia
Madalina Dumitriu , United Kingdom
Premraj Durairaj , India
Saeed Eftekhari Azam, USA
Said El Kafhali , Morocco
Antonio Elipse , Spain
R. Emre Erkmen, Canada
John Escobar , Colombia
Leandro F. F. Miguel , Brazil
FRANCESCO FOTI , Italy
Andrea L. Facci , Italy
Shahla Faisal , Pakistan
Giovanni Falsone , Italy
Hua Fan, China
Jianguang Fang, Australia
Nicholas Fantuzzi , Italy
Muhammad Shahid Farid , Pakistan
Hamed Farooqi, Iran
Yann Favennec, France
Fiorenzo A. Fazzolari , United Kingdom
Giuseppe Fedele , Italy
Roberto Fedele , Italy
Baowei Feng , China
Mohammad Ferdows , Bangladesh
Arturo J. Fernández , Spain
Jesus M. Fernandez Oro, Spain
Francesco Ferrise, Italy
Eric Feulvarch , France
Thierry Floquet, France

Eric Florentin , France
Gerardo Flores, Mexico
Antonio Forcina , Italy
Alessandro Formisano, Italy
Francesco Franco , Italy
Elisa Francomano , Italy
Juan Frausto-Solis, Mexico
Shujun Fu , China
Juan C. G. Prada , Spain
HECTOR GOMEZ , Chile
Matteo Gaeta , Italy
Mauro Gaggero , Italy
Zoran Gajic , USA
Jaime Gallardo-Alvarado , Mexico
Mosè Gallo , Italy
Akemi Gálvez , Spain
Maria L. Gandarias , Spain
Hao Gao , Hong Kong
Xingbao Gao , China
Yan Gao , China
Zhiwei Gao , United Kingdom
Giovanni Garcea , Italy
José García , Chile
Harish Garg , India
Alessandro Gasparetto , Italy
Stylianios Georgantzinou, Greece
Fotios Georgiades , India
Parviz Ghadimi , Iran
Ştefan Cristian Gherghina , Romania
Georgios I. Giannopoulos , Greece
Agathoklis Giaralis , United Kingdom
Anna M. Gil-Lafuente , Spain
Ivan Giorgio , Italy
Gaetano Giunta , Luxembourg
Jefferson L.M.A. Gomes , United Kingdom
Emilio Gómez-Déniz , Spain
Antonio M. Gonçalves de Lima , Brazil
Qunxi Gong , China
Chris Goodrich, USA
Rama S. R. Gorla, USA
Veena Goswami , India
Xunjie Gou , Spain
Jakub Grabski , Poland

Antoine Grall , France
George A. Gravvanis , Greece
Fabrizio Greco , Italy
David Greiner , Spain
Jason Gu , Canada
Federico Guarracino , Italy
Michele Guida , Italy
Muhammet Gul , Turkey
Dong-Sheng Guo , China
Hu Guo , China
Zhaoxia Guo, China
Yusuf Gurefe, Turkey
Salim HEDDAM , Algeria
ABID HUSSANAN, China
Quang Phuc Ha, Australia
Li Haitao , China
Petr Hájek , Czech Republic
Mohamed Hamdy , Egypt
Muhammad Hamid , United Kingdom
Renke Han , United Kingdom
Weimin Han , USA
Xingsi Han, China
Zhen-Lai Han , China
Thomas Hanne , Switzerland
Xinan Hao , China
Mohammad A. Hariri-Ardebili , USA
Khalid Hattaf , Morocco
Defeng He , China
Xiao-Qiao He, China
Yanchao He, China
Yu-Ling He , China
Ramdane Hedjar , Saudi Arabia
Jude Hemanth , India
Reza Hemmati, Iran
Nicolae Herisanu , Romania
Alfredo G. Hernández-Díaz , Spain
M.I. Herreros , Spain
Eckhard Hitzer , Japan
Paul Honeine , France
Jaromir Horacek , Czech Republic
Lei Hou , China
Yingkun Hou , China
Yu-Chen Hu , Taiwan
Yunfeng Hu, China

Can Huang , China
Gordon Huang , Canada
Linsheng Huo , China
Sajid Hussain, Canada
Asier Ibeas , Spain
Orest V. Iftime , The Netherlands
Przemyslaw Ignaciuk , Poland
Giacomo Innocenti , Italy
Emilio Insfran Pelozo , Spain
Azeem Irshad, Pakistan
Alessio Ishizaka, France
Benjamin Ivorra , Spain
Breno Jacob , Brazil
Reema Jain , India
Tushar Jain , India
Amin Jajarmi , Iran
Chiranjibe Jana , India
Łukasz Jankowski , Poland
Samuel N. Jator , USA
Juan Carlos Jáuregui-Correa , Mexico
Kandasamy Jayakrishna, India
Reza Jazar, Australia
Khalide Jbilou, France
Isabel S. Jesus , Portugal
Chao Ji , China
Qing-Chao Jiang , China
Peng-fei Jiao , China
Ricardo Fabricio Escobar Jiménez , Mexico
Emilio Jiménez Macías , Spain
Maolin Jin, Republic of Korea
Zhuo Jin, Australia
Ramash Kumar K , India
BHABEN KALITA , USA
MOHAMMAD REZA KHEDMATI , Iran
Viacheslav Kalashnikov , Mexico
Mathiyalagan Kalidass , India
Tamas Kalmar-Nagy , Hungary
Rajesh Kaluri , India
Jyotheeswara Reddy Kalvakurthi, India
Zhao Kang , China
Ramani Kannan , Malaysia
Tomasz Kapitaniak , Poland
Julius Kaplunov, United Kingdom
Konstantinos Karamanos, Belgium
Michal Kawulok, Poland

Irfan Kaymaz , Turkey
Vahid Kayvanfar , Qatar
Krzysztof Kecik , Poland
Mohamed Khader , Egypt
Chaudry M. Khalique , South Africa
Mukhtaj Khan , Pakistan
Shahid Khan , Pakistan
Nam-Il Kim, Republic of Korea
Philipp V. Kiryukhantsev-Korneev ,
Russia
P.V.V Kishore , India
Jan Koci , Czech Republic
Ioannis Kostavelis , Greece
Sotiris B. Kotsiantis , Greece
Frederic Kratz , France
Vamsi Krishna , India
Edyta Kucharska, Poland
Krzysztof S. Kulpa , Poland
Kamal Kumar, India
Prof. Ashwani Kumar , India
Michal Kunicki , Poland
Cedrick A. K. Kwuimy , USA
Kyandoghere Kyamakya, Austria
Ivan Kyrchei , Ukraine
Márcio J. Lacerda , Brazil
Eduardo Lalla , The Netherlands
Giovanni Lancioni , Italy
Jaroslaw Latalski , Poland
Hervé Laurent , France
Agostino Lauria , Italy
Aimé Lay-Ekuakille , Italy
Nicolas J. Leconte , France
Kun-Chou Lee , Taiwan
Dimitri Lefebvre , France
Eric Lefevre , France
Marek Lefik, Poland
Yaguo Lei , China
Kauko Leiviskä , Finland
Ervin Lenzi , Brazil
ChenFeng Li , China
Jian Li , USA
Jun Li , China
Yueyang Li , China
Zhao Li , China

Zhen Li , China
En-Qiang Lin, USA
Jian Lin , China
Qibin Lin, China
Yao-Jin Lin, China
Zhiyun Lin , China
Bin Liu , China
Bo Liu , China
Heng Liu , China
Jianxu Liu , Thailand
Lei Liu , China
Sixin Liu , China
Wanquan Liu , China
Yu Liu , China
Yuanchang Liu , United Kingdom
Bonifacio Llamazares , Spain
Alessandro Lo Schiavo , Italy
Jean Jacques Loiseau , France
Francesco Lolli , Italy
Paolo Lonetti , Italy
António M. Lopes , Portugal
Sebastian López, Spain
Luis M. López-Ochoa , Spain
Vassilios C. Loukopoulos, Greece
Gabriele Maria Lozito , Italy
Zhiguo Luo , China
Gabriel Luque , Spain
Valentin Lychagin, Norway
YUE MEI, China
Junwei Ma , China
Xuanlong Ma , China
Antonio Madeo , Italy
Alessandro Magnani , Belgium
Toqeer Mahmood , Pakistan
Fazal M. Mahomed , South Africa
Arunava Majumder , India
Sarfraz Nawaz Malik, Pakistan
Paolo Manfredi , Italy
Adnan Maqsood , Pakistan
Muazzam Maqsood, Pakistan
Giuseppe Carlo Marano , Italy
Damijan Markovic, France
Filipe J. Marques , Portugal
Luca Martinelli , Italy
Denizar Cruz Martins, Brazil

Francisco J. Martos , Spain
Elio Masciari , Italy
Paolo Massioni , France
Alessandro Mauro , Italy
Jonathan Mayo-Maldonado , Mexico
Pier Luigi Mazzeo , Italy
Laura Mazzola, Italy
Driss Mehdi , France
Zahid Mehmood , Pakistan
Roderick Melnik , Canada
Xiangyu Meng , USA
Jose Merodio , Spain
Alessio Merola , Italy
Mahmoud Mesbah , Iran
Luciano Mescia , Italy
Laurent Mevel , France
Constantine Michailides , Cyprus
Mariusz Michta , Poland
Prankul Middha, Norway
Aki Mikkola , Finland
Giovanni Minafò , Italy
Edmondo Minisci , United Kingdom
Hiroyuki Mino , Japan
Dimitrios Mitsotakis , New Zealand
Ardashir Mohammadzadeh , Iran
Francisco J. Montáns , Spain
Francesco Montefusco , Italy
Gisele Mophou , France
Rafael Morales , Spain
Marco Morandini , Italy
Javier Moreno-Valenzuela , Mexico
Simone Morganti , Italy
Caroline Mota , Brazil
Aziz Moukrim , France
Shen Mouquan , China
Dimitris Mourtzis , Greece
Emiliano Mucchi , Italy
Taseer Muhammad, Saudi Arabia
Ghulam Muhiuddin, Saudi Arabia
Amitava Mukherjee , India
Josefa Mula , Spain
Jose J. Muñoz , Spain
Giuseppe Muscolino, Italy
Marco Mussetta , Italy

Hariharan Muthusamy, India
Alessandro Naddeo , Italy
Raj Nandkeolyar, India
Keivan Navaie , United Kingdom
Soumya Nayak, India
Adrian Neagu , USA
Erivelton Geraldo Nepomuceno , Brazil
AMA Neves, Portugal
Ha Quang Thinh Ngo , Vietnam
Nhon Nguyen-Thanh, Singapore
Papakostas Nikolaos , Ireland
Jelena Nikolic , Serbia
Tatsushi Nishi, Japan
Shanzhou Niu , China
Ben T. Nohara , Japan
Mohammed Nouari , France
Mustapha Nourelfath, Canada
Kazem Nouri , Iran
Ciro Núñez-Gutiérrez , Mexico
Włodzimierz Ogryczak, Poland
Roger Ohayon, France
Krzysztof Okarma , Poland
Mitsuhiro Okayasu, Japan
Murat Olgun , Turkey
Diego Oliva, Mexico
Alberto Olivares , Spain
Enrique Onieva , Spain
Calogero Orlando , Italy
Susana Ortega-Cisneros , Mexico
Sergio Ortobelli, Italy
Naohisa Otsuka , Japan
Sid Ahmed Ould Ahmed Mahmoud , Saudi Arabia
Taoreed Owolabi , Nigeria
EUGENIA PETROPOULOU , Greece
Arturo Pagano, Italy
Madhumangal Pal, India
Pasquale Palumbo , Italy
Dragan Pamučar, Serbia
Weifeng Pan , China
Chandan Pandey, India
Rui Pang, United Kingdom
Jürgen Pannek , Germany
Elena Panteley, France
Achille Paolone, Italy

George A. Papakostas , Greece
Xosé M. Pardo , Spain
You-Jin Park, Taiwan
Manuel Pastor, Spain
Pubudu N. Pathirana , Australia
Surajit Kumar Paul , India
Luis Payá , Spain
Igor Pažanin , Croatia
Libor Pekař , Czech Republic
Francesco Pellicano , Italy
Marcello Pellicciari , Italy
Jian Peng , China
Mingshu Peng, China
Xiang Peng , China
Xindong Peng, China
Yuxing Peng, China
Marzio Pennisi , Italy
Maria Patrizia Pera , Italy
Matjaz Perc , Slovenia
A. M. Bastos Pereira , Portugal
Wesley Peres, Brazil
F. Javier Pérez-Pinal , Mexico
Michele Perrella, Italy
Francesco Pesavento , Italy
Francesco Petrini , Italy
Hoang Vu Phan, Republic of Korea
Lukasz Pieczonka , Poland
Dario Piga , Switzerland
Marco Pizzarelli , Italy
Javier Plaza , Spain
Goutam Pohit , India
Dragan Poljak , Croatia
Jorge Pomares , Spain
Hiram Ponce , Mexico
Sébastien Poncet , Canada
Volodymyr Ponomaryov , Mexico
Jean-Christophe Ponsart , France
Mauro Pontani , Italy
Sivakumar Poruran, India
Francesc Pozo , Spain
Aditya Rio Prabowo , Indonesia
Anchasa Pramuanjaroenkij , Thailand
Leonardo Primavera , Italy
B Rajanarayan Prusty, India

Krzysztof Puszynski , Poland
Chuan Qin , China
Dongdong Qin, China
Jianlong Qiu , China
Giuseppe Quaranta , Italy
DR. RITU RAJ , India
Vitomir Racic , Italy
Carlo Rainieri , Italy
Kumbakonam Ramamani Rajagopal, USA
Ali Ramazani , USA
Angel Manuel Ramos , Spain
Higinio Ramos , Spain
Muhammad Afzal Rana , Pakistan
Muhammad Rashid, Saudi Arabia
Manoj Rastogi, India
Alessandro Rasulo , Italy
S.S. Ravindran , USA
Abdolrahman Razani , Iran
Alessandro Reali , Italy
Jose A. Reinoso , Spain
Oscar Reinoso , Spain
Haijun Ren , China
Carlo Renno , Italy
Fabrizio Renno , Italy
Shahram Rezapour , Iran
Ricardo Riaza , Spain
Francesco Riganti-Fulginei , Italy
Gerasimos Rigatos , Greece
Francesco Ripamonti , Italy
Jorge Rivera , Mexico
Eugenio Roanes-Lozano , Spain
Ana Maria A. C. Rocha , Portugal
Luigi Rodino , Italy
Francisco Rodríguez , Spain
Rosana Rodríguez López, Spain
Francisco Rossomando , Argentina
Jose de Jesus Rubio , Mexico
Weiguo Rui , China
Rubén Ruiz , Spain
Ivan D. Rukhlenko , Australia
Dr. Eswaramoorthi S. , India
Weichao SHI , United Kingdom
Chaman Lal Sabharwal , USA
Andrés Sáez , Spain

Bekir Sahin, Turkey
Laxminarayan Sahoo , India
John S. Sakellariou , Greece
Michael Sakellariou , Greece
Salvatore Salamone, USA
Jose Vicente Salcedo , Spain
Alejandro Salcido , Mexico
Alejandro Salcido, Mexico
Nunzio Salerno , Italy
Rohit Salgotra , India
Miguel A. Salido , Spain
Sinan Salih , Iraq
Alessandro Salvini , Italy
Abdus Samad , India
Sovan Samanta, India
Nikolaos Samaras , Greece
Ramon Sancibrian , Spain
Giuseppe Sanfilippo , Italy
Omar-Jacobo Santos, Mexico
J Santos-Reyes , Mexico
José A. Sanz-Herrera , Spain
Musavarah Sarwar, Pakistan
Shahzad Sarwar, Saudi Arabia
Marcelo A. Savi , Brazil
Andrey V. Savkin, Australia
Tadeusz Sawik , Poland
Roberta Sburlati, Italy
Gustavo Scaglia , Argentina
Thomas Schuster , Germany
Hamid M. Sedighi , Iran
Mijanur Rahaman Seikh, India
Tapan Senapati , China
Lotfi Senhadji , France
Junwon Seo, USA
Michele Serpilli, Italy
Silvestar Šesnić , Croatia
Gerardo Severino, Italy
Ruben Sevilla , United Kingdom
Stefano Sfarra , Italy
Dr. Ismail Shah , Pakistan
Leonid Shaikhet , Israel
Vimal Shanmuganathan , India
Prayas Sharma, India
Bo Shen , Germany
Hang Shen, China

Xin Pu Shen, China
Dimitri O. Shepelsky, Ukraine
Jian Shi , China
Amin Shokrollahi, Australia
Suzanne M. Shontz , USA
Babak Shotorban , USA
Zhan Shu , Canada
Angelo Sifaleras , Greece
Nuno Simões , Portugal
Mehakpreet Singh , Ireland
Piyush Pratap Singh , India
Rajiv Singh, India
Seralathan Sivamani , India
S. Sivasankaran , Malaysia
Christos H. Skiadas, Greece
Konstantina Skouri , Greece
Neale R. Smith , Mexico
Bogdan Smolka, Poland
Delfim Soares Jr. , Brazil
Alba Sofi , Italy
Francesco Soldovieri , Italy
Raffaele Solimene , Italy
Yang Song , Norway
Jussi Sopanen , Finland
Marco Spadini , Italy
Paolo Spagnolo , Italy
Ruben Specogna , Italy
Vasilios Spitas , Greece
Ivanka Stamova , USA
Rafał Stanisławski , Poland
Miladin Stefanović , Serbia
Salvatore Strano , Italy
Yakov Strelniker, Israel
Kangkang Sun , China
Qiuqin Sun , China
Shuaishuai Sun, Australia
Yanchao Sun , China
Zong-Yao Sun , China
Kumarasamy Suresh , India
Sergey A. Suslov , Australia
D.L. Suthar, Ethiopia
D.L. Suthar , Ethiopia
Andrzej Swierniak, Poland
Andras Szekrenyes , Hungary
Kumar K. Tamma, USA

Yong (Aaron) Tan, United Kingdom
Marco Antonio Taneco-Hernández , Mexico
Lu Tang , China
Tianyou Tao, China
Hafez Tari , USA
Alessandro Tasora , Italy
Sergio Teggi , Italy
Adriana del Carmen Téllez-Anguiano , Mexico
Ana C. Teodoro , Portugal
Efsthathios E. Theotokoglou , Greece
Jing-Feng Tian, China
Alexander Timokha , Norway
Stefania Tomasiello , Italy
Gisella Tomasini , Italy
Isabella Torcicollo , Italy
Francesco Tornabene , Italy
Mariano Torrisi , Italy
Thang nguyen Trung, Vietnam
George Tsiatas , Greece
Le Anh Tuan , Vietnam
Nerio Tullini , Italy
Emilio Turco , Italy
Ilhan Tuzcu , USA
Efstratios Tzirtzilakis , Greece
FRANCISCO UREÑA , Spain
Filippo Ubertini , Italy
Mohammad Uddin , Australia
Mohammad Safi Ullah , Bangladesh
Serdar Ulubeyli , Turkey
Mati Ur Rahman , Pakistan
Panayiotis Vafeas , Greece
Giuseppe Vairo , Italy
Jesus Valdez-Resendiz , Mexico
Eusebio Valero, Spain
Stefano Valvano , Italy
Carlos-Renato Vázquez , Mexico
Martin Velasco Villa , Mexico
Franck J. Vernerey, USA
Georgios Veronis , USA
Vincenzo Vespri , Italy
Renato Vidoni , Italy
Venkatesh Vijayaraghavan, Australia

Anna Vila, Spain
Francisco R. Villatoro , Spain
Francesca Vipiana , Italy
Stanislav Vitek , Czech Republic
Jan Vorel , Czech Republic
Michael Vynnycky , Sweden
Mohammad W. Alomari, Jordan
Roman Wan-Wendner , Austria
Bingchang Wang, China
C. H. Wang , Taiwan
Dagang Wang, China
Guoqiang Wang , China
Huaiyu Wang, China
Hui Wang , China
J.G. Wang, China
Ji Wang , China
Kang-Jia Wang , China
Lei Wang , China
Qiang Wang, China
Qingling Wang , China
Weiwei Wang , China
Xinyu Wang , China
Yong Wang , China
Yung-Chung Wang , Taiwan
Zhenbo Wang , USA
Zhibo Wang, China
Waldemar T. Wójcik, Poland
Chi Wu , Australia
QiuHong Wu, China
Yuqiang Wu, China
Zhibin Wu , China
Zhizheng Wu , China
Michalis Xenos , Greece
Hao Xiao , China
Xiao Ping Xie , China
Qingzheng Xu , China
Binghan Xue , China
Yi Xue , China
Joseph J. Yame , France
Chuanliang Yan , China
Xinggang Yan , United Kingdom
Hongtai Yang , China
Jixiang Yang , China
Mijia Yang, USA
Ray-Yeng Yang, Taiwan

Zaoli Yang , China
Jun Ye , China
Min Ye , China
Luis J. Yebra , Spain
Peng-Yeng Yin , Taiwan
Muhammad Haroon Yousaf , Pakistan
Yuan Yuan, United Kingdom
Qin Yuming, China
Elena Zaitseva , Slovakia
Arkadiusz Zak , Poland
Mohammad Zakwan , India
Ernesto Zambrano-Serrano , Mexico
Francesco Zammori , Italy
Jessica Zangari , Italy
Rafal Zdunek , Poland
Ibrahim Zeid, USA
Nianyin Zeng , China
Junyong Zhai , China
Hao Zhang , China
Haopeng Zhang , USA
Jian Zhang , China
Kai Zhang, China
Lingfan Zhang , China
Mingjie Zhang , Norway
Qian Zhang , China
Tianwei Zhang , China
Tongqian Zhang , China
Wenyu Zhang , China
Xianming Zhang , Australia
Xuping Zhang , Denmark
Yinyan Zhang, China
Yifan Zhao , United Kingdom
Debao Zhou, USA
Heng Zhou , China
Jian G. Zhou , United Kingdom
Junyong Zhou , China
Xueqian Zhou , United Kingdom
Zhe Zhou , China
Wu-Le Zhu, China
Gaetano Zizzo , Italy
Mingcheng Zuo, China

Contents

Variable Mass Control and Parameter Identification of Spacecraft Orbit Refueling Process

Xu Han , Zhi Li , Hui Li , Longfei Huang , and Yujia Pang 

Research Article (17 pages), Article ID 9660218, Volume 2022 (2022)

Research Article

Variable Mass Control and Parameter Identification of Spacecraft Orbit Refueling Process

Xu Han ¹, Zhi Li ¹, Hui Li ², Longfei Huang ¹ and Yujia Pang ¹

¹Qian Xuesen Laboratory of Space Technology of China Academy of Space Technology, Beijing 100094, China

²Zhongbing Navigation Control Technology Group Co, Ltd, Beijing 100081, China

Correspondence should be addressed to Xu Han; hanxu@qxslab.cn

Received 17 June 2021; Accepted 17 February 2022; Published 13 June 2022

Academic Editor: Lei Wang

Copyright © 2022 Xu Han et al. This is an open access article distributed under the Creative Commons Attribution License, which permits unrestricted use, distribution, and reproduction in any medium, provided the original work is properly cited.

A maintainable refueling vehicle is the future development direction of the space system. In the process of fuel filling, capture docking, and configuration transformation, the most significant factor that affects the attitude control of the system is the continuous or sudden change of the angular torque of the system. In this paper, we study the control system of the variable mass body in an on-orbit service in the process of configuration transformation. The large errors of torque of inertia may make the narrow sense TEA (torque equilibrium attitude) of the system deviate greatly from the earth-oriented attitude. In order to avoid the error caused by the partial linearization of the system model, the feedback linearization method of the nonlinear system is used to design the controller to realize the tracking of the narrow sense TEA in the process of configuration transformation. Different from the traditional attitude control method, in order to avoid the high cost of the control system caused by the change of system mass characteristics and the change of system angular torque, CMG (control moment gyroscope) angular torque is introduced into the controller. We design a joint controller of attitude control and angular torque management, which can effectively stabilize the system and reduce the angular torque saturation of the attitude control system during the on-orbit service.

1. Introduction

Low cost, high reliability, fast response, and maintainability are the development direction of the future space system. The function of on-orbit refueling may become the design requirement of future spacecraft. The on-orbit refueling mission is a part of the space service support system, which takes the on-orbit spacecraft with insufficient fuel, exhausted fuel, or propulsion system failure as the application object. By means of cabin addition, fuel filling, or module replacement, the function of the spacecraft propulsion system can be supplemented or restored, and the mission capability of spacecraft on-orbit can be improved or extended. The on-orbit refueling mission consists of two parts: the replenishment vehicle and the replenished vehicle.

The on-orbit refueling process usually includes (1) the capture and docking process of the replenishment vehicle and the replenished vehicle to realize the combination connection of the two vehicles and (2) the fuel filling and

transfer process after the fuel tank connection. In the process of fuel filling, capture docking, and configuration change, the biggest influence on the attitude control of the system is the constant change or mutation of the angular torque of the system, especially when CMG is used as the actuator. The CMG needs to be unloaded by air jet. Because CMG absorbs the momentum of the system change quickly to saturation. And the control structure coupling is easily caused by the unloading of the jet during this period, which makes the control condition worse.

The variable mass control problems of spacecraft during the refueling process can be divided into three categories: the variable mass control problems of the spacecraft docking process, the variable mass control problems of the refueling process, and the variable mass control problems of the spacecraft separation process. The change of system mass in the process of fuel transfer can be regarded as continuous, while the system mass changes suddenly in the process of capture docking and separation. Taking the system

configuration change whose mass change rate is between the above two as an example, the control of the variable mass body is studied.

Wu et al. [1] used the hybrid method to study the attitude stability of small satellites, in order to solve the problem of excessive output of the controller. Chu et al. [2] developed an approximate dynamic model with uncertain parameters considering the uncertainty of model parameters and proposed a robust adaptive control strategy to compensate for or reject these uncertainties, respectively. Huang and Uang [3] aimed at the problems of various disturbances and parameter changes encountered in the process of the spacecraft space mission, the sliding film control was applied to PID control, and the two were combined to complete the spacecraft attitude robust control. Qin [4] proposed a controller design method for singularly perturbed systems. Zhou and Zeng [5] proposed a new nonlinear robust H_∞ control method for spacecraft attitude maneuver problems with external disturbances and perturbed disturbances. Yuan et al. [6] proposed a decoupling control algorithm based on a robust adaptive method to solve the problem of spacecraft attitude control with disturbance and torque of inertia uncertainty. Tong and Li [7] proposed a static output feedback controller using multiobjective synthesis technology and studied the robust stability and disturbance suppression of spacecraft with parameter variation and control input saturation constraints. However, this method does not consider the uncertainties of the attachment frequency and rigid-flexible coupling matrix. Yang et al. [8] studied the orbit robust control of low earth orbit spacecraft under the condition of parameter variation during orbit transfer during rendezvous. Liang et al. [9] planned the angular trajectory of the satellite's attitude maneuver around the Euler axis and designed a variable structure control law based on the error quaternion and error angular velocity between the actual and planned positions of the satellite. Based on the time-varying autoregressive sliding average model and the good local function fitting ability of the wavelet basis function, Lei et al. [10] used the Mexican cap wavelet function as the spatial base of the time-varying coefficients of the TARMA model and constructed a time-varying autoregressive sliding average model of the functional series based on the wavelet function. And decoupling estimation of time-varying coefficients is achieved.

In this paper, from the angle of system angular torque, the angular torque of the system is introduced into the control system, and the angular torque and attitude of the system are jointly controlled to achieve a good balance between the attitude and angular torque of the system and ensure that the system is stable in a certain equilibrium attitude, and the angular torque of the system will not be saturated due to the change of the mass characteristics of the system. The joint control of attitude and angular torque is referred to as attitude control/angular torque management (ACMM).

2. Problem Formulation

2.1. Simplified System Model. The replenishment vehicle operates the replenished vehicle with a manipulator. Taking

the configuration transformation process of the resupplied aircraft from "I" configuration to "L" configuration as an example, the model is established.

Assuming that the solar panels are locked and the slow variables are ignored, the system dynamics model of the configuration transformation process is as follows:

$$\mathbf{I}_s(t)\dot{\boldsymbol{\omega}}_s + \dot{\mathbf{I}}_s(t)\boldsymbol{\omega}_s + \mathbf{R}_{bl}\dot{\boldsymbol{\omega}}_{bl} + \boldsymbol{\omega}_s^\times \mathbf{I}_s(t)\boldsymbol{\omega}_s + \boldsymbol{\omega}_s^\times \mathbf{R}_{bl}\boldsymbol{\omega}_{bl} + \sum_{i=1}^n \ddot{\mathbf{F}}_{si}\boldsymbol{\eta}_{ai} = \mathbf{T}_s. \quad (1)$$

$$\ddot{\boldsymbol{\eta}}_{ai} + 2\zeta_{ai}\boldsymbol{\Omega}_{ai}\dot{\boldsymbol{\eta}}_{ai} + \boldsymbol{\Omega}_{ai}^2\boldsymbol{\eta}_{ai} + \mathbf{F}_{ti}^T\ddot{\mathbf{X}} + \mathbf{F}_{si}^T\dot{\boldsymbol{\omega}}_s + \mathbf{F}_{ai}^T\dot{\boldsymbol{\omega}}_{ai} + \mathbf{F}_{li}^T\dot{\boldsymbol{\omega}}_{bl} = \mathbf{0}. \quad (2)$$

Among them, formula (1) is the attitude dynamics equation of the central rigid body, and formula (2) is the vibration equation of the solar panel. $\mathbf{I}_s(t)$ is the expression of the instantaneous torque of inertia of the combination in the body coordinate system (\mathbf{F}_s). The specific expression is as follows:

$$\mathbf{I}_s(t) = \mathbf{I}_b^b + \mathbf{I}_l^r - m((r_{bl}^s)^\times)^2, \quad (3)$$

where \mathbf{I}_b^b is the torque of inertia of the replenishment vehicle relative to its body coordinate system. \mathbf{I}_l^r is the representation of the torque of inertia of the replenished aircraft in its reference coordinate system. Let the torque of inertia of the replenished vehicle can be expressed as \mathbf{I}_l^l in the body coordinate system, and the transformation matrix between the body coordinate system and the reference coordinate system is $\mathbf{L}_{(Ir)(Ib)}$, and then,

$$\mathbf{I}_l^r = \mathbf{L}_{(Ir)(Ib)}\mathbf{I}_l^l\mathbf{L}_{(Ir)(Ib)}^T. \quad (4)$$

$\boldsymbol{\omega}_s$ is the component representation of the angular rate of rotation of the system relative to the inertial frame in the body assembly coordinate system. r_{bl}^b is the component representation of the vector from the centroid of the replenishment vehicle to the centroid of the replenished vehicle in the body coordinate system of the assembly. m is the reduced mass of the two-body system. If the mass of the replenishment vehicle and the replenished vehicle is m_b and m_l , respectively, the reduced mass can be expressed as follows:

$$m = \frac{m_b m_l}{m_b + m_l}. \quad (5)$$

$\boldsymbol{\omega}_{bl}$ is the rotational angular velocity of the replenished vehicle relative to the replenished vehicle, that is, the relative attitude angular velocity, which is described in the body coordinate system of the assembly. \mathbf{R}_{bl} is the motion coupling coefficient of the replenishment vehicle and the replenished vehicle, which is expressed in the body assembly coordinate system. \mathbf{F}_{li} is the coupling coefficient between the solar panel and the rotational motion of the replenished vehicle, which is expressed in the system of the replenished vehicle.

$\mathbf{F}_{ai}\mathbf{F}_{si}$ are the coupling coefficient matrix of solar panel rotation and satellite rotation. $\boldsymbol{\eta}$ represents the displacement

caused by the force. \mathbf{F}_i is the principal vector array of system forces.

When there is no confusion, the subscript s is omitted to identify the system parameter, and the coordinate system of the variable is clearly marked. Let ω_{AB} be the angular velocity vector of a coordinate system relative to the B coordinate system. When B coordinate system is the inertial system, B is omitted. For example, \mathbf{X}_A^B is the component representation of \mathbf{X}_A in the B coordinate system. The torque of inertia \mathbf{I}_s , the angular velocity of inertia ω_s , and control torque \mathbf{T}_s in the centroid coordinate system of the system are abbreviated as \mathbf{I}^b , ω^b , and \mathbf{T}^b , respectively.

In the process of configuration transformation, the dynamic equation and environmental torque model of CMG are consistent with that of long-term normal on-orbit flight. The final system model for controller design is as follows [11]:

Attitude dynamics:

$$\mathbf{I}^b(t)\dot{\omega}^b = \mathbf{T}_c^b + \mathbf{T}_{\text{gyro}}^b + \mathbf{T}_{\text{dl}}^b + \mathbf{T}_j^b + \mathbf{T}_g^b + \mathbf{T}_d^b, \quad (6)$$

where ω^b is the angular velocity of inertia; \mathbf{I}^b is the torque of inertia; \mathbf{T}_c^b is the output torque of CMG; $\mathbf{T}_{\text{gyro}}^b$ is the gyro coupling torque; \mathbf{T}_{dl}^b is the perturbation torque of the supplied vehicle; \mathbf{T}_g^b is the gravity gradient torque; \mathbf{T}_d^b is the atmospheric disturbance torque.

Let $F_o(o_0x_0y_0z_0)$ be the orbital coordinate system, and $F_b(o_bx_by_bz_b)$ be the body coordinate system. The attitude kinematics model can be expressed as follows:

$$\begin{bmatrix} \omega_x^b \\ \omega_y^b \\ \omega_z^b \end{bmatrix} = \begin{bmatrix} \dot{\varphi}c\theta - \dot{\psi}c\varphi s\theta \\ \dot{\theta} + \dot{\psi}s\varphi \\ \dot{\psi}s\theta + \dot{\varphi}c\varphi c\theta \end{bmatrix} - \begin{bmatrix} \omega_0(s\psi c\theta + s\varphi s\theta c\psi) \\ \omega_0 c\psi c\varphi \\ -\omega_0(s\varphi c\theta c\psi - s\psi s\theta) \end{bmatrix}, \quad (7)$$

where ψ , φ , θ are the yaw, roll, and pitch angles of the aircraft, respectively. “ s ” and “ c ” represent “sin” and “cos” functions, respectively. ω_x^b , ω_y^b , and ω_z^b represent the triaxial component of the absolute angular velocity ω^b of the combination in the coordinate system F_b , and ω_0 is the orbital angular velocity. It is assumed that ω_0 is constant when the assembly runs in a circular orbit.

The CMG kinetic model is as follows:

$$-\dot{\mathbf{h}}_c^b - (\omega^b)^\times \mathbf{h}_c^b = \mathbf{T}_c^b, \quad (8)$$

where \mathbf{h}_c^b is the sum of the absolute angular torque of each CMG to its own center of mass, which is described in the body coordinate system of the combination; \mathbf{T}_c^b is the attitude control torque of CMG.

When the attitude of the system satisfies the following equation, all kinds of torques can be balanced.

$$-(\omega^b)^\times \mathbf{I}^b(t)(\omega^b)^* + \mathbf{T}_{\text{dl}}^b + \mathbf{T}_g^b + \mathbf{T}_d^b = 0. \quad (9)$$

If the controller is designed to make the attitude of the combination track the TEA under this condition, the configuration transformation operation can be completed without unloading the angular torque of CMG. However,

due to the complexity of configuration transformation, TEA is difficult to solve. And because of the rapid change of TEA in this process, large space structures are generally not suitable for rapid maneuver. So, the attitude control strategy of tracking dynamic TEA in the configuration transformation process is not feasible.

The time of configuration transformation is shorter than that of the normal flight in orbit, and the angular torque accumulation caused by aerodynamic torque is much smaller than that caused by gravitational gradient torque and perturbation torque. Although the perturbation torque is one of the main reasons for CMG angular torque accumulation, the perturbation angular torque in different stages of the transfer process can cancel each other to a great extent after the path and velocity of the manipulator are reasonably planned. Therefore, in the preliminary design of the controller, the influence of aerodynamic torque and perturbation torque can be ignored temporarily. In this case, only the gravitational gradient torque and the orbital gyroscopic torque are considered, and the attitude satisfying the following form during configuration transformation is defined as “narrow sense TEA.”

$$-(\omega^b)^\times \mathbf{I}^b(t)(\omega^b)^* + \mathbf{T}_g^b = 0. \quad (10)$$

In the process of configuration transformation, the purpose of ACMM controller design is to make the system track the narrow sense TEA. The physical meaning of TEA in the orbit system is obvious when only considering the gravitational gradient torque and the orbital gyroscopic torque. Therefore, the controller design of this part is carried out in the orbit system, which is not only convenient for the derivation of feedback linearization control law but also can further study the characteristics of TEA in the orbit system [12].

2.2. Mechanical Model

2.2.1. Attitude Dynamics Equation. The derivative of coordinate transformation matrix from body coordinate system to orbit system is as follows:

$$\dot{\mathbf{L}}_{\text{ob}} = \mathbf{\Omega}_{\text{bo}}^o \mathbf{L}_{\text{ob}}, \quad (11)$$

where $\mathbf{\Omega}_{\text{bo}}^o = (\omega_b^o - \eta)^\times$.

In the process of configuration transformation, the torque of inertia of the system changes constantly, but without confusion, the time mark is omitted. The relationship between the torque of inertia of the system in the body coordinate system and the orbit system is as follows:

$$\mathbf{I}^o = \mathbf{L}_{\text{ob}} \mathbf{I}^b \mathbf{L}_{\text{bo}}, \quad (12)$$

$$\dot{\mathbf{I}}_b^o = \mathbf{\Omega}_{\text{bo}}^o \mathbf{I}_b^o - \mathbf{I}_b^o \mathbf{\Omega}_{\text{bo}}^o. \quad (13)$$

The component of the absolute angular velocity of the combination in the orbit system is expressed as follows:

$$\omega^o = \mathbf{L}_{\text{ob}} \omega^b. \quad (14)$$

By deriving the time from equation (14) and using equation (10), the system dynamic equation described in the orbit system is obtained.

$$\dot{\omega}^o = (\mathbf{I}^o)^{-1} \left((\omega^o)^\times \mathbf{I}^o \omega^o + 3\omega_0^2 (\hat{R}^o \times \mathbf{I}^o \hat{R}^o) + \mathbf{T}_c^o \right) + \mathbf{T}_d^o. \quad (15)$$

2.2.2. Attitude Kinematics Equation. Note that $\Theta_{ob} = [\varphi_{ob} \ \theta_{ob} \ \psi_{ob}]^T$ is the Euler angle from the body coordinate system to the orbit system. In the case of no confusion, omit the lower corner mark indicating the direction of rotation. Using 3-1-2 transformation order, the kinematics equation of the system in the orbit system is as follows:

$$\dot{\Theta}_{ob} = \mathbf{R}_\omega^o \omega^o + \boldsymbol{\eta}, \quad (16)$$

$$\text{where } \mathbf{R}_\omega^o = - (1/\cos \varphi) \begin{bmatrix} \cos \varphi \cos \theta & 0 & \cos \varphi \sin \theta \\ \sin \varphi \sin \theta & \cos \varphi & -\sin \varphi \sin \theta \\ -\sin \theta & 0 & \cos \theta \end{bmatrix}.$$

2.2.3. CMG Kinetic Equation. The dynamic equation of CMG angular torque in the orbit system is as follows:

$$\dot{\mathbf{h}}_c^o = -(\omega^o)^\times \mathbf{h}_c^o - \mathbf{T}_c^o. \quad (17)$$

2.2.4. ACMM System Design Model. Equations (15)–(17) are written as state equations, and the system model for controller design is obtained as

$$\begin{bmatrix} \dot{\Theta}_{ob} \\ \dot{\omega}^o \\ \dot{\mathbf{h}}_c^o \end{bmatrix} = \begin{bmatrix} \mathbf{R}_\omega^o \omega^o + \boldsymbol{\eta} \\ (\mathbf{I}^o)^{-1} \left((\omega^o)^\times \mathbf{I}^o \omega^o + 3\omega_0^2 (\hat{R}^o \times \mathbf{I}^o \hat{R}^o) \right) \\ -(\omega^o)^\times \mathbf{h}_c^o \end{bmatrix} + \begin{bmatrix} 0_3 \\ (\mathbf{I}^o)^{-1} \mathbf{T}_c^o \\ 0_3 \end{bmatrix} + \begin{bmatrix} 0_3 \\ (\mathbf{I}^o)^{-1} \mathbf{T}_d^o \end{bmatrix}. \quad (18)$$

3. Control System Design based on Adaptive Feedback Linearization

In the process of configuration transformation, the large change of torque of inertia may make the narrow sense TEA of the system deviate greatly from the earth-oriented attitude. In order to avoid the error caused by the partial linearization of the system model, the feedback linearization method of the nonlinear system is used to design the controller to realize the tracking of the narrow sense TEA. In the process of configuration transformation, the large change of torque of inertia may make the narrow sense TEA of the system deviate greatly from the earth-oriented attitude. In order to avoid the error caused by the partial linearization of the system model, the feedback linearization method of the nonlinear system is used to design the

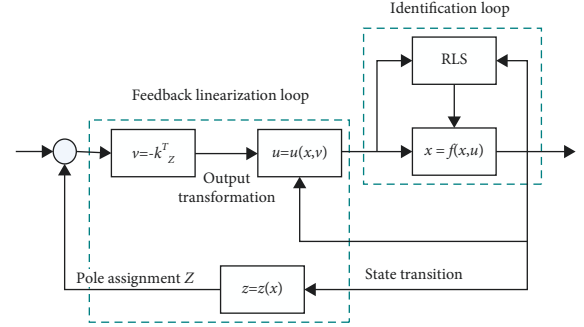


FIGURE 1: Structure diagram of adaptive feedback linearization controller.

controller to realize the tracking of the narrow sense TEA in the process of configuration transformation.

The core idea of feedback linearization is to make the nonlinear system realize accurate linearization of state or input/output under certain conditions through appropriate nonlinear state transformation and feedback transformation, so as to transform the nonlinear system design problem into a linear system design problem. It is different from the traditional method of local linearization using Taylor expansion [13], which does not ignore any nonlinear term in the linearization process, so this method is not only accurate but also holistic; that is, linearization is applicable to the whole region of the transformation. The limitation of this method is that it needs accurate information of the system. When the parameters are uncertain, it is unable to carry out accurate feedback linearization.

In order to compensate for the dependence of the feedback linearization method on system parameters, an adaptive ACMM controller with online parameter identification is designed. The controller consists of two parts: online parameter identification loop and feedback linearization control loop. The structure diagram is shown in Figure 1 [14].

3.1. Feedback Linearization Analysis. Under the assumption of a small angle, the coordinate transformation matrix from F_b to F_o can be approximately expressed as

$$\mathbf{L}_{ob} = \mathbf{I} - \boldsymbol{\Theta}_{ob}^\times, \quad (19)$$

where \mathbf{E}_3 is the 3×3 unit matrix and $\boldsymbol{\Theta}_{ob}^\times$ is the antisymmetric matrix of $\boldsymbol{\Theta}_{ob}$, $\boldsymbol{\Theta}_{ob}^\times = \begin{bmatrix} 0 & -\psi & \theta \\ \psi & 0 & -\varphi \\ -\theta & \varphi & 0 \end{bmatrix}$.

The results are as follows:

$$\begin{aligned} \mathbf{I}^o &= (\mathbf{E}_3 - \boldsymbol{\Theta}_{ob}^\times) \mathbf{I}^b (\mathbf{E}_3 + \boldsymbol{\Theta}_{ob}^\times) \approx \mathbf{I}^b - \boldsymbol{\Theta}_{ob}^\times \mathbf{I}^b + \mathbf{I}^b \boldsymbol{\Theta}_{ob}^\times, \\ (\mathbf{I}^o)^{-1} &\approx (\mathbf{I}^b)^{-1} - \boldsymbol{\Theta}_{ob}^\times (\mathbf{I}^b)^{-1} + (\mathbf{I}^b)^{-1} \boldsymbol{\Theta}_{ob}^\times. \end{aligned} \quad (20)$$

Taking the system state variable as $\mathbf{x} = [\Theta_{ob} \ \omega^o \ \mathbf{h}_c^o]^T$, the state equation is written as a general nonlinear system

$$\dot{\mathbf{x}} \triangleq \mathbf{f}(\mathbf{x}) + \mathbf{G}(\mathbf{x})\mathbf{u}, \quad (21)$$

where $\mathbf{x} \in R^9$, $\mathbf{u} \in R^3$,

$$\mathbf{f}(\mathbf{x}) = [\mathbf{R}_\omega^o \omega^o + \boldsymbol{\eta}(\mathbf{I}^o)^{-1}((\omega^o)^\times \mathbf{I}^o \omega^o + 3\omega_0^2(\tilde{\mathbf{R}}^o \times \mathbf{I}^o \tilde{\mathbf{R}}^o)) - (\omega^o)^\times \mathbf{h}_c^o]^T, \quad (22)$$

$$\mathbf{G}(\mathbf{x}) = \begin{bmatrix} \mathbf{0}_3 & (\mathbf{I}^o)^{-1} & -\mathbf{E}_3 \end{bmatrix}^T, \quad \mathbf{u} = \mathbf{T}_c^o. \quad (23)$$

$$\begin{aligned} \mathbf{G}_0(\mathbf{x}) &= \text{span}\{\mathbf{g}_1(\mathbf{x}) \ \mathbf{g}_2(\mathbf{x}) \ \mathbf{g}_3(\mathbf{x})\}, \\ \mathbf{G}_1(\mathbf{x}) &= \text{span}\{\mathbf{g}_1(\mathbf{x}) \ \mathbf{g}_2(\mathbf{x}) \ \mathbf{g}_3(\mathbf{x}) \ \text{ad}_f \mathbf{g}_1(\mathbf{x}) \ \text{ad}_f \mathbf{g}_2(\mathbf{x}) \ \text{ad}_f \mathbf{g}_3(\mathbf{x})\}, \\ &\dots \\ \mathbf{G}_i(\mathbf{x}) &= \text{span}\{\text{ad}_f^k \mathbf{g}_j(\mathbf{x}): 0 \leq k \leq i, 1 \leq j \leq 3\}, \quad i = 1, \dots, 8, \end{aligned} \quad (24)$$

where span represents vector expansion; that is, $\mathbf{G}_0(\mathbf{x})$ represents subspace formed by a linear combination of $\mathbf{g}_1(\mathbf{x}) \ \mathbf{g}_2(\mathbf{x}) \ \mathbf{g}_3(\mathbf{x})$, $\text{ad}_f^k \mathbf{g}(x) = [f, \text{ad}_f^{k-1} \mathbf{g}](x)$. Where $[]$ is Lie brackets, $[f, g](x) = (\partial g / \partial x) f(x) - (\partial f / \partial x) g(x)$, $\mathbf{h}_{c0}^o = \begin{pmatrix} 0 & h_{cy}^o & 0 \end{pmatrix}$, $\mathbf{x}_0 = \begin{pmatrix} 0 & \boldsymbol{\eta} & \mathbf{h}_{c0}^o \end{pmatrix}^T$ can be used to test.

When $1 \leq i \leq 8$, the distribution $\mathbf{G}_i(\mathbf{x})$ is a constant dimension in the neighborhood of \mathbf{x}_0 .

When $1 \leq i \leq 7$, the distribution $\mathbf{G}_i(\mathbf{x})$ is involutivity.

The distribution $\mathbf{G}_i(\mathbf{x})$ has dimension 9.

According to the exact feedback linearization theorem, the system can be linearized by exact feedback. Therefore, three output variables with total relative order 9 can be used to define the state transformation, and the system can be transformed into a standard canonical form. Since the total relative order of the system is equal to the state dimension of the system, all states can be observed through the input-output relationship.

3.2. State Transition. The state transformation is defined by the Lie derivative of the output variable. For the ACMM system, in order to avoid angular torque accumulation effectively under the premise of attitude stability, CMG angular torque and attitude stability information should be taken as output variables at the same time.

$$\mathbf{H}_b^o = \mathbf{h}_c^o + \mathbf{I}^o \omega^o. \quad (25)$$

The second-order Lie derivative, the second-order Lie derivative, and the third-order Lie derivative, respectively, for the triaxial components of equation \mathbf{H}_b^o are obtained as

$$L_f^2 H_{b1}^o(x) = -\omega_0^2 H_{b1}^o + 3\omega_0^2 I_{yz}^o, \quad (26)$$

$$L_f^2 H_{b2}^o(x) = 3\omega_0^2 I_{yz}^o, \quad (27)$$

$$L_f^2 H_{b3}^o(x) = -\omega_0^3 H_{b1}^o - 3\omega_0^2 I_{yz}^o. \quad (28)$$

It can be seen from equation (12) that \mathbf{I}^o contains angular velocity information, and the control torque information

The whole state of the system can be measured, and when $\|\mathbf{I}^o\| \neq 0$, $\mathbf{f}(\mathbf{x})$, $\mathbf{G}(\mathbf{x})$ is continuous and smooth.

Substituting the approximate expression equation (15) of $(\mathbf{I}^o)^{-1}$ into the expression (23) of $\mathbf{G}(\mathbf{x})$, denote $\mathbf{G}(\mathbf{x}) = [\mathbf{g}_1(\mathbf{x}) \ \mathbf{g}_2(\mathbf{x}) \ \mathbf{g}_3(\mathbf{x})]$. Definition:

will appear after further derivation. Therefore, according to equations (26)–(28), the third derivative of H_{b1}^o , H_{b2}^o and the fourth derivative of H_{b3}^o will appear control torque information, which can be used as output variables.

In order to meet the relative order requirements of the system, the magnitude after derivation is unified, the accuracy of numerical calculation is improved, and the output variables are selected as follows:

$$\begin{aligned} y_1 &= H_{b3}^o(x), \\ y_2 &= \omega_0 H_{b2}^o(x), \\ y_3 &= 3\omega_0^3 I_{xy}^o(x). \end{aligned} \quad (29)$$

The nonlinear transformation of output variable definition is as follows:

$$\mathbf{z} = \Phi(\mathbf{x}), \quad (30)$$

where $\mathbf{z}^T = (\mathbf{z}_1^T \ \mathbf{z}_2^T \ \mathbf{z}_3^T)$, $\mathbf{x}^T = (\boldsymbol{\Theta}_{ob}^T \ (\omega^o)^T \ (h_c^o)^T)^T$.

The specific form of nonlinear transformation is as follows:

$$\begin{aligned} z_{11} &= H_{b3}^o(x), \\ z_{12} &= L_f H_{b3}^o(x) = -\omega_0^2 H_{b1}^o, \\ z_{13} &= L_f^2 H_{b3}^o(x) = -3\omega_0^3 I_{yz}^o - \omega_0^2 H_{b3}^o, \\ z_{14} &= L_f^3 H_{b3}^o(x) \\ &= -3\omega_0^3 \{ (I_y^o - I_z^o) \omega_x^2 + I_{xy}^o (\omega_y^2 + \omega_0) - I_{xz}^o \omega_z^2 \} + \omega_0^3 H_{b1}^o, \\ z_{21} &= \omega_0 H_{b2}^o(x), \\ z_{22} &= L_f (\omega_0 H_{b2}^o(x)) = -3\omega_0^2 I_{xz}^o, \\ z_{23} &= L_f^2 (\omega_0 H_{b2}^o(x)) \\ &= 3\omega_0^3 \{ -I_{xy}^o \omega_x^2 + (I_z^o - I_x^o) (\omega_y^2 + \omega_0) + I_{yz}^o \omega_z^2 \}, \end{aligned} \quad (31)$$

(32)

$$\begin{aligned} z_{31} &= 3\omega_0^3 I_{xy}^o(x), \\ z_{32} &= L_f(3\omega_0^3 \Pi_{xy}^o(x)) \\ &= 3\omega_0^3 \{-I_{xz}^o \omega_x^o + I_{yz}^o(\omega_y^o + \omega_0) - (I_x^o - I_y^o)\omega_z^o\}. \end{aligned} \quad (33)$$

The new equation of state is as follows:

$$\begin{aligned} \dot{z}_{11} &= z_{12}, \dot{z}_{12} = z_{13}, \dot{z}_{13} = z_{14}, \\ \dot{z}_{21} &= z_{22}, \dot{z}_{22} = z_{23}, \dot{z}_{31} = z_{32}, \end{aligned} \quad (34)$$

$$\begin{bmatrix} \dot{z}_{14} \\ \dot{z}_{23} \\ \dot{z}_{32} \end{bmatrix} = \begin{bmatrix} L_f^4 y_1 \\ L_f^3 y_2 \\ L_f^2 y_3 \end{bmatrix} + \begin{bmatrix} L_{g1} L_f^3 y_1 & L_{g2} L_f^3 y_1 & L_{g3} L_f^3 y_1 \\ L_{g1} L_f^2 y_2 & L_{g2} L_f^2 y_2 & L_{g3} L_f^2 y_2 \\ L_{g1} L_f y_3 & L_{g2} L_f y_3 & L_{g3} L_f y_3 \end{bmatrix} \begin{bmatrix} u_1^o \\ u_2^o \\ u_3^o \end{bmatrix}. \quad (35)$$

Let $\mathbf{z}^* = [z_{14} \ z_{23} \ z_{32}]^T$, (35) be written as follows:

$$\dot{\mathbf{z}}^* \triangleq \mathbf{f}^*(x) + \mathbf{E}(x)\mathbf{u}^o. \quad (36)$$

The definitions of $\mathbf{f}^*(x)$ and decoupling matrix $\mathbf{E}(x)$ are obvious.

$$\begin{aligned} \mathbf{E}(x) &= -3\omega_0^3 \mathbf{S}_1^o (\mathbf{I}^o)^{-1}, \\ \mathbf{f}^*(x) &= \mathbf{c} + 3\omega_0^2 [\mathbf{S}_1^o (\boldsymbol{\omega}^o \times \boldsymbol{\eta}) + \mathbf{S}_2^o (\boldsymbol{\omega}^o - \boldsymbol{\eta}) - (\boldsymbol{\omega}^o - \boldsymbol{\eta}) \times \mathbf{S}_1^o (\boldsymbol{\omega}^o - \boldsymbol{\eta}) + \\ &\quad \mathbf{S}_1^o (\mathbf{I}^o)^{-1} \{-(\boldsymbol{\omega}^o)^\times \mathbf{I}^o \boldsymbol{\omega}^o + 3\omega_0^2 (\hat{\mathbf{R}}^o \times \mathbf{I}^o \mathbf{R}^o)\}], \end{aligned} \quad (37)$$

$$\text{where} \quad \mathbf{S}_1^o = \begin{bmatrix} I_y^o - I_z^o & I_{xy}^o & -I_{xz}^o \\ -I_{xy}^o & I_z^o - I_x^o & I_{yz}^o \\ I_{xz}^o & -I_{yz}^o & I_x^o - I_y^o \end{bmatrix}, \quad \mathbf{S}_2^o = \begin{bmatrix} I_y^o - I_z^o & 0 & 0 \\ 0 & I_z^o - I_x^o & 0 \\ 0 & 0 & I_x^o - I_y^o \end{bmatrix}, \quad \mathbf{c} = \begin{bmatrix} -\omega_0^2 z_1 \\ 0 \\ 0 \end{bmatrix}.$$

3.3. Input Transformation. When $\mathbf{E}(x)$ is reversible, the following input transformation is adopted for the system (25):

$$\mathbf{u}^o = \mathbf{E}^{-1}(x) \begin{bmatrix} v_1 - L_f^4 H_{b3}^o(x) \\ v_2 - L_f^3 (\omega_0 H_{b2}^o(x)) \\ v_2 - L_f^2 (\omega_0^3 H_{b2}^o(x)) \end{bmatrix}. \quad (38)$$

System (25) will be equivalent to

$$\dot{\mathbf{z}}^* = \mathbf{v}, \quad (39)$$

where $\mathbf{v} = [v_1 \ v_2 \ v_3]^T$.

The system (39) has a linear input-output relationship. When its output is expected to track the desired trajectory \mathbf{z}_d without error, the corresponding linear control law can be designed.

$$\mathbf{v} = \mathbf{K}(\mathbf{z}_d - \mathbf{z}) + \dot{\mathbf{z}}_d^*, \quad (40)$$

where \mathbf{K} is the control gain matrix in the form of (40) and $\dot{\mathbf{z}}_d^*$ is the expected trajectory change rate.

$$\mathbf{K} = \begin{bmatrix} k_{11} & k_{12} & k_{13} & k_{14} & 0 & 0 & 0 & 0 & 0 \\ 0 & 0 & 0 & 0 & k_{21} & k_{22} & k_{23} & 0 & 0 \\ 0 & 0 & 0 & 0 & 0 & 0 & 0 & k_{31} & k_{32} \end{bmatrix}. \quad (41)$$

The characteristic equation of an equivalent linear system is as follows:

$$\lambda = (s^4 + k_{14}s^3 + k_{13}s^2 + k_{12}s + k_{11})(s^3 + k_{23}s^2 + k_{22}s + k_{21})(s^2 + k_{32}s + k_{31}). \quad (42)$$

According to equations (36) and (41), the nonlinear control law for the linearized system (39) is obtained.

$$\mathbf{u}^o = \mathbf{E}^{-1}(x)(-\mathbf{f}^*(x) + \mathbf{v}), \quad (43)$$

$$\begin{aligned} \mathbf{u}^o &= \mathbf{I}^o (\boldsymbol{\omega}^o \times \boldsymbol{\eta}) - (\boldsymbol{\omega}^o)^\times \mathbf{I}^o \boldsymbol{\omega}^o + 3\omega_0^2 (\hat{\mathbf{R}}^o \times \mathbf{I}^o \mathbf{R}^o) \\ &\quad - \mathbf{I}^o (\mathbf{S}_1^o)^{-1} \{(\boldsymbol{\omega}^o - \boldsymbol{\eta})\mathbf{S}_1^o (\boldsymbol{\omega}^o - \boldsymbol{\eta}) - \mathbf{S}_2^o (\boldsymbol{\omega}^o - \boldsymbol{\eta})\} \\ &\quad - \frac{1}{3\omega_0^3} \mathbf{I}^o (\mathbf{S}_1^o)^{-1} \{\dot{\mathbf{z}}_d' - \boldsymbol{\varepsilon} + \mathbf{K}(\mathbf{z}_d - \mathbf{z})\}, \end{aligned} \quad (44)$$

$$\mathbf{u}^o = \mathbf{L}_{b0} \mathbf{u}^o. \quad (45)$$

Equations (44) and (45) are the nonlinear control laws of the ACMM system in the track system. In this control law, it is assumed that the inertia characteristics of the system can be fully identified, and only the desired trajectory \mathbf{z}_d and the feedback gain matrix \mathbf{K} need to be designed.

3.4. System Expected Trajectory. The stable working state of the ACMM system is a narrow sense TEA when only considering the gravitational gradient torque. At this point, $I_{xy}^o = I_{xz}^o = I_{yz}^o = 0$, $I_x^o = I_x^p$, $I_y^o = I_y^p$, $I_z^o = I_z^p$, and $h_{cx}^o = 0$, $h_{cy}^o = 0$. The total angular torque of the system at TEA is

$$\mathbf{H}_b^o = \begin{pmatrix} 0 \\ h_c^o \\ 0 \end{pmatrix} + \begin{bmatrix} I_i^p & 0 & 0 \\ 0 & I_j^p & 0 \\ 0 & 0 & I_k^p \end{bmatrix} \begin{pmatrix} 0 \\ -\omega_0 \\ 0 \end{pmatrix} = \begin{pmatrix} 0 \\ h_c^o - I_j^p \omega_0 \\ 0 \end{pmatrix}, \quad (46)$$

where $i \neq j, j \neq k, i \neq k$, I_i^p, I_j^p, I_k^p are the value of inertia along the three principal axes of inertia.

After the total angular torque of the system at TEA is obtained, the desired trajectory \mathbf{z}_d of the system can be determined. Although TEA does not require h_{cy}^o and can take any value within the capacity range of CMG, in order to simplify the design of the controller, the instruction value of h_{cy}^o is zero. The narrow sense of TEA requires the inertial principal axis to point along the orbit coordinate axis, but in the case of minimum attitude maneuver, the inertial principal axis in the y direction is generally pointed to the normal direction of the orbit; that is, $\mathbf{H}_b^o = (0 \ -I_y^p \omega_0 \ 0)$.

From the above analysis, we can get the expected trajectory \mathbf{z}_d as follows:

$$\mathbf{z}_d = [0 \ 0 \ 0 \ 0 \ -I_y^p \omega_0 \ 0 \ 0 \ 0 \ 0]^T. \quad (47)$$

3.5. Equivalent Linear System Design. The closed-loop characteristic of the equivalent linear system is designed by the pole assignment method. In order to make the system have a certain stability margin and convergence speed, the closed-loop poles are placed in the sector area with an angle of $\pm 45^\circ$ between the left side of the S plane $S = -0.5\omega_0$ and the real axis. Select 9 closed-loop poles as $-0.5\omega_0$, $(-0.707 \pm 0.1j)\omega_0$, $(-1 \pm 0.5j)\omega_0$, $(-1.414 \pm 0.5j)\omega_0$, $(-2 \pm j)\omega_0$, and the specific distribution is shown in Figure 2.

For the fourth-order SISO system corresponding to \mathbf{z}_1 , the closed-loop poles are assigned at $(-0.707 \pm 0.1j)\omega_0$ and $(-1.414 \pm 0.5j)\omega_0$. The corresponding fourth-order characteristic equation is as follows:

$$\lambda_1(s) = s^4 + 4.24\omega_0 s^3 + 6.75\omega_0^2 s^2 + 1.77\omega_0^3 s + 2.75\omega_0^4. \quad (48)$$

Therefore, $k_{11} = 2.75\omega_0^4$, $k_{12} = 1.77\omega_0^3$, $k_{13} = 6.75\omega_0^2$, $k_{14} = 4.24\omega_0$.

For the third-order single input single output system of \mathbf{z}_2 choosing $-0.5\omega_0$ and $(-2 \pm j)\omega_0$ as its closed-loop poles, the corresponding feedback gain can be obtained in the same way $k_{21} = 2.5\omega_0^3$, $k_{22} = 7.0\omega_0^2$, $k_{23} = 4.5\omega_0$.

For the second-order single input single output system of \mathbf{z}_3 , the closed-loop pole is $(-1 \pm 0.5j)\omega_0$, and the feedback gain is calculated as $k_{31} = 1.25\omega_0^2$, $k_{32} = 2.0\omega_0$.

4. Online Parameter Identification

It can be seen from the feedback control law (39) that the ACMM controller needs not only the angular rate and angular torque information of the combined body but also its torque of inertia information, which is provided by the online parameter identification unit, and its identification accuracy directly affects the control performance of the adaptive system. In this section, the control torque information and angular velocity information of the combination

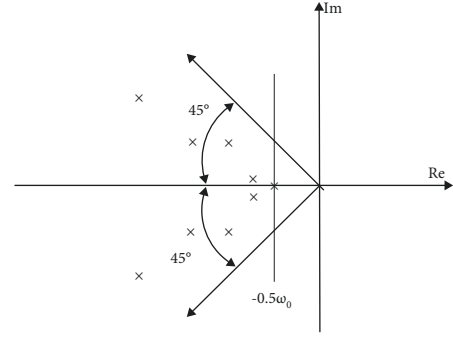


FIGURE 2: Pole assignment diagram of the equivalent linear system.

are used to identify the closed-loop control of the combination without additional excitation. The algorithm uses the least square method with a bounded gain forgetting factor, which can track the real parameters without continuous excitation.

The standard form of the linear least squares [15] problem is $\Phi\mathbf{x} = \mathbf{y} + \varepsilon$ or written as $\Phi\mathbf{x} \cong \mathbf{y}$, where \mathbf{y} is the measured vector, ε is the measured noise vector, \mathbf{x} is the parameter to be identified, Φ is composed of known variables and parameters, and $\hat{\mathbf{x}}$ is the solution of the least-squares algorithm, which minimizes the sum of squares of error $\Phi\hat{\mathbf{x}} - \mathbf{y}$.

Firstly, the least square estimation model of the parameters to be identified is constructed according to the dynamic equation of the system, and the vector composed of six independent elements of the torque of inertia is taken as the unknown vector $\mathbf{i} = [I_x^o \ I_y^o \ I_z^o \ I_{xy}^o \ I_{xz}^o \ I_{yz}^o]^T$.

$$\begin{aligned} \mathbf{I}^o \boldsymbol{\omega}^o &= \mathbf{D}_1(\dot{\boldsymbol{\omega}}^o) \mathbf{i}, \\ (\boldsymbol{\omega}^o)^\times \mathbf{I}^o \boldsymbol{\omega}^o &= \mathbf{D}_2(\boldsymbol{\omega}^o) \mathbf{i}, \end{aligned} \quad (49)$$

where

$$\begin{aligned} \mathbf{D}_1(\dot{\boldsymbol{\omega}}) &= \begin{bmatrix} \dot{\omega}_x^o & 0 & 0 & 0 & \dot{\omega}_z^o & \dot{\omega}_y^o \\ 0 & \dot{\omega}_y^o & 0 & \dot{\omega}_z^o & 0 & \dot{\omega}_x^o \\ 0 & 0 & \dot{\omega}_z^o & \dot{\omega}_y^o & \dot{\omega}_x^o & 0 \end{bmatrix}, \\ \mathbf{D}_2(\boldsymbol{\omega}) &= \begin{bmatrix} 0 & -\omega_y^o \omega_z^o & \omega_y^o \omega_z^o & (\omega_y^o)^2 - (\omega_z^o)^2 & \omega_x^o \omega_y^o & -\omega_x^o \omega_z^o \\ \omega_x^o \omega_z^o & 0 & -\omega_x^o \omega_z^o & -\omega_x^o \omega_y^o & (\omega_z^o)^2 - (\omega_x^o)^2 & \omega_y^o \omega_z^o \\ -\omega_x^o \omega_y^o & \omega_x^o \omega_y^o & 0 & \omega_x^o \omega_z^o & -\omega_y^o \omega_z^o & (\omega_x^o)^2 - (\omega_y^o)^2 \end{bmatrix}. \end{aligned} \quad (50)$$

The system dynamics equation in the orbit system can be reduced to the following equation:

$$\mathbf{D}_1(\dot{\boldsymbol{\omega}}^o) \mathbf{i} + \mathbf{D}_2(\boldsymbol{\omega}^o) \mathbf{i} - 3\omega_0^2 \mathbf{D}_2(\hat{\mathbf{R}}) \mathbf{i} = \mathbf{T}_c^o + \mathbf{T}_d^o. \quad (51)$$

Since the angular acceleration information is not measurable and the angular velocity information is measurable, the left and right sides of equation (51) are integrated to obtain the following results:

$$\left(\mathbf{D}_1 \left(\boldsymbol{\omega}^o \middle|_{t_0}^{t_1} \right) + \int_{t_0}^{t_1} (\mathbf{D}_2(\boldsymbol{\omega}^o) - 3\omega_0^2 \mathbf{D}_2(\hat{R})) dt \right) \mathbf{i} = \int_{t_0}^{t_1} (\mathbf{T}_c^o + \mathbf{T}_d^o) dt. \quad (52)$$

If equation (52) is written in the form of standard linear least squares, then

$$\begin{aligned} \Phi &= \mathbf{D}_1 \left(\boldsymbol{\omega}^o \middle|_{t_0}^{t_1} \right) + \int_{t_0}^{t_1} (\mathbf{D}_2(\boldsymbol{\omega}^o) - 3\omega_0^2 \mathbf{D}_2(\hat{R})) dt, \\ \mathbf{y} &= \int_{t_0}^{t_1} (\mathbf{T}_c^o + \mathbf{T}_d^o) dt. \end{aligned} \quad (53)$$

In order to realize online real-time identification, the recursive form of least squares is used. Recursive least square estimation extracts the information of the estimated quantity from each measurement, which is used to modify the estimation obtained in the previous step [16]. The more times of measurement, the more times of correction, and the higher the accuracy of estimation.

When the system is brought into TEA, the external force torques cancel each other, and the control torque required is small, which cannot meet the continuous excitation conditions required by the traditional least square method. Moreover, due to the “data saturation” phenomenon, when the observation data increase, the deviation between the estimated value obtained by the recursive least square parameter identification method and the real parameters will become larger and larger. Therefore, in parameter estimation, we should pay enough attention to the current data and gradually forget the old data which does not contain the current dynamic characteristics, so we use the recursive least squares estimator with bounded gain forgetting factor. The estimator still has bounded gain when the excitation is not continuous [17].

Set \mathbf{X} to be measured, \mathbf{Y}_j is the j measurement, and the measurement equation is

$$\mathbf{Y}_j = \Phi_j \mathbf{X} + \mathbf{V}_j, \quad j = 1, 2, \dots, k, \quad (54)$$

where Φ_j and \mathbf{V}_j are the j measurement matrix and random measurement noise. The recursive least square estimation algorithm with the forgetting factor is as follows:

$$\begin{aligned} \mathbf{K}_k &= (\lambda \mathbf{E} + \Phi_{k+1} \mathbf{P}_k \Phi_{k+1}^T)^{-1}, \\ \mathbf{P}_{k+1} &= \frac{1}{\lambda} (\mathbf{P}_k - \mathbf{P}_k \Phi_{k+1}^T \mathbf{K}_k \Phi_{k+1} \mathbf{P}_k), \\ \hat{\mathbf{X}}_{k+1} &= \hat{\mathbf{X}}_k + \mathbf{P}_{k+1} \Phi_{k+1}^T (\mathbf{Z}_{k+1} - \Phi_{k+1} \hat{\mathbf{X}}_k). \end{aligned} \quad (55)$$

The choice of forgetting factor is of great significance to the stability of the system. When the continuous excitation is satisfied (such as in the dynamic process of tracking TEA), the forgetting factor of zero will lead to zero gain (i.e., it degenerates to the standard least squares method, resulting in the instability of tracking time-varying parameters) [18]. When the continuous excitation condition is not satisfied, the forgetting factor of the normal number will lead to a

sharp increase in gain. The forgetting factor is chosen as the following bounded form:

$$\lambda(t) = \lambda_0 \left(1 - \frac{\|\mathbf{P}\|}{k_0} \right). \quad (56)$$

λ_0 and k_0 is a normal number. The upper bounds of the maximum forgetting rate and the norm of the gain matrix are given, respectively; \mathbf{P} is the gain matrix and represents the level of motivation. Formula (56) means when the norm of \mathbf{P} is small (strong continuous incentive), the forgetting factor is λ_0 , forgetting is fast, and the system has a strong ability to track the changing parameters. When the norm of \mathbf{P} increases, the forgetting speed decreases. And the forgetting speed is zero when the norm of \mathbf{P} reaches a specified upper bound. In this case, λ_0 is 0.95, and k_0 is 10^9 .

5. Controllability and Singularity

The nonlinear state transformation (34)–(36) are not global transformation. They are effective at the nonsingular points of the matrix in the new state equation. Nonsingular points are effective. In this case, the inverse matrix is

$$\mathbf{E}^{-1}(t) = -\frac{1}{3\omega_0^2} \mathbf{I}^o (\mathbf{S}_1^o)^{-1}. \quad (57)$$

Formula (57) shows that the reversibility of $\mathbf{E}(x)$ depends on the reversibility of \mathbf{S}_1^o . According to the definition of \mathbf{S}_1^o , its reversibility is determined by the following formula:

$$\begin{aligned} \Delta &= \det(\mathbf{S}_1^o) = (I_x^o - I_y^o)(I_y^o - I_z^o)(I_z^o - I_x^o) \\ &\quad + (I_x^o - I_y^o)(I_{xz}^o)^2 + (I_z^o - I_x^o)(I_{xz}^o)^2 + (I_y^o - I_z^o)(I_{yz}^o)^2. \end{aligned} \quad (58)$$

Due to the existence of the torque of inertia of the inertial coordinate system of the system mass center and the track system, the following relations are

$$\mathbf{I}^o = \mathbf{L}_{op} \mathbf{I}^p \mathbf{L}_{po}. \quad (59)$$

Δ can be changed to

$$\Delta = (I_x^p - I_y^p)(I_y^p - I_z^p)(I_z^p - I_x^p) \Lambda(\varphi^*, \theta^*, \Psi^*). \quad (60)$$

This is a function of the rotation Euler angle (narrow sense TEA) from the center of mass inertial principal axis coordinate system to the orbit system when the 3-1-2 rotation sequence is adopted, and the simplified expression of $\Lambda(\varphi^*, \theta^*, \Psi^*)$ is as follows:

$$\begin{aligned} \Lambda(\varphi^*, \theta^*, \Psi^*) &= \cos(2\varphi^*) \cos(2\theta^*) \cos(2\Psi^*) \\ &\quad + \frac{1}{4} \sin(2\varphi^*) \sin(2\theta^*) \sin(2\Psi^*) (1 - 3 \cos(2\varphi^*)). \end{aligned} \quad (61)$$

When the following two conditions are met, $\Delta \neq 0$

$$\begin{aligned} I_x^p &\neq I_y^p \neq I_z^p, I_x^p \neq I_z^p \neq I_y^p, \\ \Lambda &\neq 0. \end{aligned} \quad (62)$$

Among them, the first condition is a physical condition, which restricts the inertia characteristics of the system and can feedback linearization. The second condition limits the attitude range of the control law (43).

5.1. Torque of Inertia Constraint. Inertia constraints $I_x^p \neq I_y^p \neq I_z^p$ are the inherent characteristic of the ACMM problem which only considers the gravity gradient torque, and even for the linear controller, the same constraint is needed. For example, assuming that the nonlinear dynamic equations of the system are linearized at zero attitude, the dynamic equations of pitch and roll/yaw in the ACMM system are decoupled. For pitch channel, take the state variable as $x_2 = (\theta^* \dot{\theta}^* h_c^p)^T$, the equation of state is

$$\dot{x}_2 = \mathbf{A}_2 \mathbf{x} + \mathbf{b}_2 u_2^p, \quad (63)$$

where

$$\mathbf{A}_2 = \frac{1}{I_y^p} \begin{bmatrix} 0 & I_y^p & 0 \\ 3\omega_0^2(I_z^p - I_x^p) & 0 & 0 \\ 0 & 0 & 0 \end{bmatrix}, \quad (64)$$

$$\mathbf{b}_2 = \frac{1}{I_y^p} \begin{pmatrix} 0 \\ -1 \\ I_y^p \end{pmatrix}.$$

The controllable matrix is:

$$\mathbf{S} = \frac{1}{(I_y^p)^2} \begin{bmatrix} 0 & -I_y^p & 0 \\ -I_y^p & 0 & 3\omega_0^2(I_z^p - I_x^p) \\ (I_y^p)^2 & 0 & 0 \end{bmatrix}. \quad (65)$$

When $I_z^p \neq I_x^p$, $\text{rank}(\mathbf{S}) = 2 < 3$. The pitch axis is uncontrollable, and the roll/yaw axis has a similar conclusion.

5.2. Attitude Constraint. The nonlinear control law (39) requires $\Lambda \neq 0$. In order to avoid singularity, it is necessary to study the distribution of attitude angle when $\Lambda = 0$. When using the 3-1-2 rotation sequence, according to the expression of Λ , and $I_x^p \neq I_y^p \neq I_z^p$, $I_z^p \neq I_x^p$, the singular surface near $\Theta^* = (0 \ 0 \ 0)$ is obtained, as shown in Figure 3.

The two surfaces in Figures 4 and 5 will separate the TEA at $\theta^* = (0, 0, 0)$ from other TEA. If the initial attitude of the system is located in the area surrounded by the surface in the figure, it cannot pass through the surface in the process of tracking TEA, so as to avoid the singularity of the nonlinear control law.

Because Λ a function of three attitude angles, it is hard to observe Λ with the change of attitude angle. Considering that the change of yaw angle is more obvious in the process of configuration transformation, and the gravitational

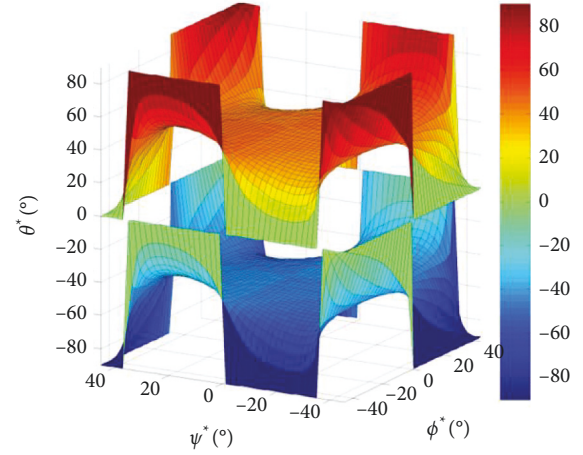


FIGURE 3: Singular surface of the control law.

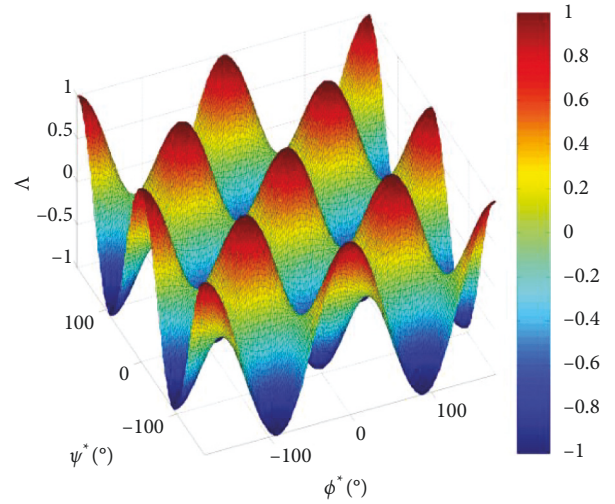


FIGURE 4: Value of Λ when $\varphi^* = 0^\circ$.

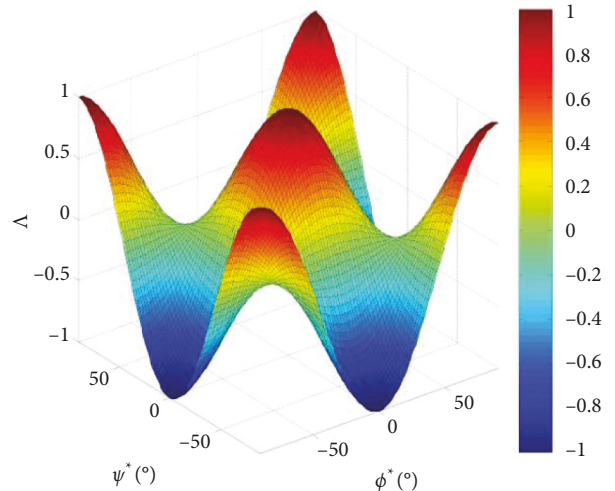
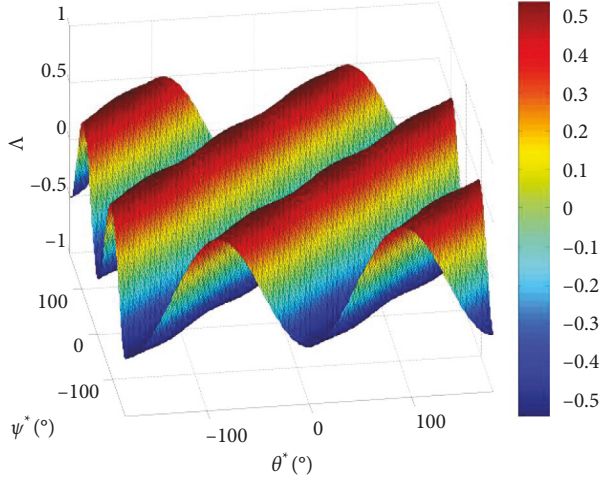
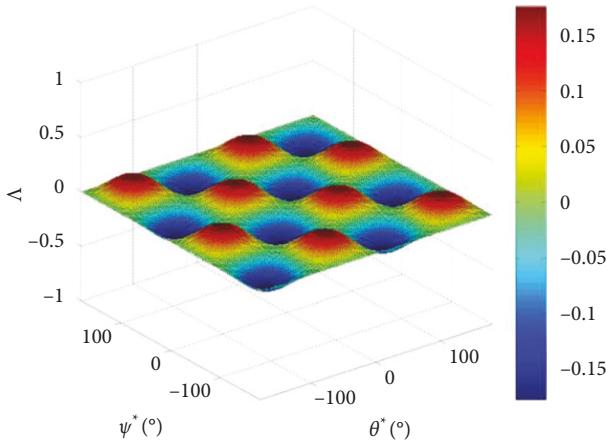


FIGURE 5: Value of Λ when $\varphi^* = 0^\circ$ (close up view).

FIGURE 6: The value of Λ when $\varphi^* = -90^\circ$.FIGURE 7: The value of Λ when $\varphi^* = -45^\circ$.

gradient torque is generally more obvious in the pitch axis, the roll angle is fixed here to investigate the influence of pitch angle and yaw angle on Λ .

Figures 6 and 7 show the value of Λ when $\varphi^* = 0$, $\theta^*, \psi^* \in [-180^\circ, 180^\circ]$. As can be seen from the figure, $\varphi^* = 0$, corresponding to the balanced attitude

$$\Theta^* = \left(\frac{m\pi}{2} \quad \frac{n\pi}{2} \quad 0 \right), \quad (66)$$

where the value of Λ is $(-1)^{m+n}$, and it is local maximum 1 or local minimum -1. When $\varphi^* = 0$, $\theta^* = \pm 45^\circ$, $\psi^* = \pm 45^\circ$, $\Lambda = 0$, so if the initial time $\theta^* < 45^\circ$, $\psi^* < 45^\circ$, $\varphi = 0$, the uniqueness TEA $\theta = (0, 0, 0)$ that can be achieved by a combination not passing through the singular surface of $\Lambda = 0$ in a graph. The value of Λ is 1.

Figures 6 to 13 show that when φ^* changes from -90° to 90° , Λ changes with the θ^*, ψ^* . This set of curves shows that the value of Λ is symmetrically distributed with respect to $\theta^* = \psi^*$ and $\theta^* = -\psi^*$. When φ^* increased from -90° to -45° , along $\theta^* = \psi^*$, it is constant. But along the $\theta^* = -\psi^*$, the amplitude of the fluctuation of Λ becomes smaller, as shown in the figure. When φ^* increased to -45° , a single peak

and trough appeared; when φ^* increased from -45° to 0° , the amplitude of wave crest and wave trough becomes larger; when $\varphi^* = 0$, the peak and trough values reach the maximum value of 1 and the minimum value of -1, respectively; when φ^* increased from 0 to 45° , the amplitudes of wave crest and wave trough decrease, respectively; when φ^* increased from 45° to 90° , Λ is symmetric about $\theta^* = \psi^*$ and $\theta^* = -\psi^*$ again. However, Λ rotates at 90° degrees. When $\theta^* = -\psi^*$, Λ is a constant.

It can be seen from the previous analysis that when only considering the gravitational gradient torque, the narrow sense TEA has the following form:

$$\Theta^* = \left(\frac{m\pi}{2} \quad \frac{n\pi}{2} \quad \frac{p\pi}{2} \right). \quad (67)$$

Before applying the nonlinear control law, the distance between TEA and the singular point must be determined. The nonlinear control law is effective only when Λ at TEA is far from zero.

Take the first and second partial derivatives of Λ :

$$\frac{\partial \Lambda}{\partial \Theta^*} = \left[\frac{\partial \Lambda}{\partial \varphi^*} \quad \frac{\partial \Lambda}{\partial \theta^*} \quad \frac{\partial \Lambda}{\partial \psi^*} \right]^T, \quad (68)$$

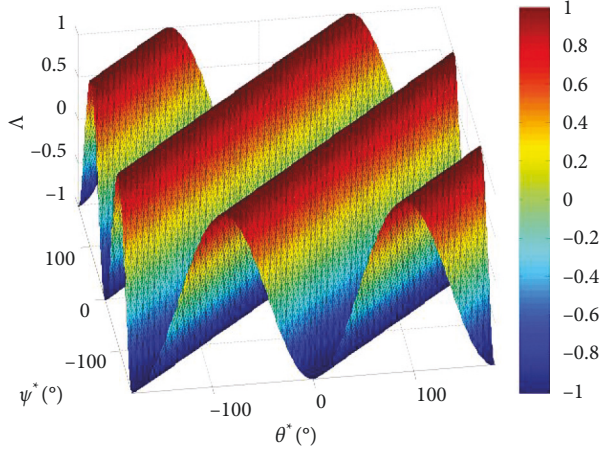
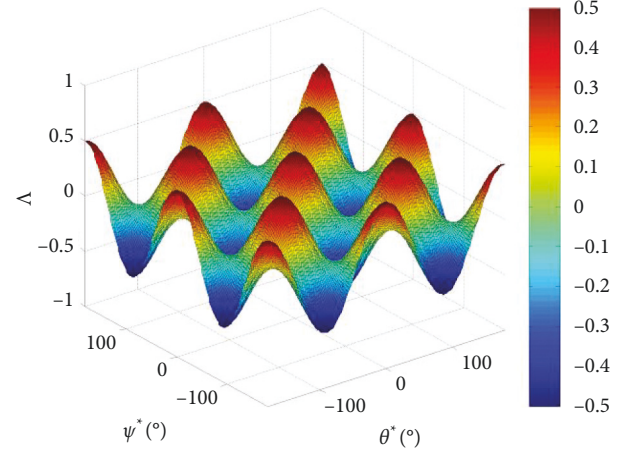
where

$$\begin{aligned} \frac{\partial \Lambda}{\partial \varphi^*} &= -2 \sin(2\varphi^*) \cos(2\theta^*) \cos(2\psi^*) \\ &+ \frac{1}{4} \sin(2\theta^*) \sin(2\psi^*) [\cos(\varphi^*) (1 - 3 \cos(2\varphi^*)) \\ &+ 6 \sin(\varphi^*) \sin(2\varphi^*)], \end{aligned}$$

$$\begin{aligned} \frac{\partial \Lambda}{\partial \theta^*} &= -2 \cos(2\varphi^*) \sin(2\theta^*) \cos(2\psi^*) \\ &+ \frac{1}{2} \cos(2\theta^*) \sin(2\psi^*) \sin(\varphi^*) (1 - 3 \cos(2\varphi^*)), \end{aligned}$$

$$\begin{aligned} \frac{\partial \Lambda}{\partial \psi^*} &= -2 \cos(2\varphi^*) \cos(2\theta^*) \sin(2\psi^*) \\ &+ \frac{1}{2} \sin(2\theta^*) \cos(2\psi^*) \sin(\varphi^*) (1 - 3 \cos(2\varphi^*)), \end{aligned}$$

$$\frac{\partial \Lambda}{\partial \Theta^{*2}} = \begin{bmatrix} \frac{\partial \Lambda}{\partial \varphi^{*2}} & \frac{\partial \Lambda}{\partial \varphi^* \partial \theta^*} & \frac{\partial \Lambda}{\partial \varphi^* \partial \psi^*} \\ \frac{\partial \Lambda}{\partial \varphi^* \partial \theta^*} & \frac{\partial \Lambda}{\partial \theta^{*2}} & \frac{\partial \Lambda}{\partial \theta^* \partial \psi^*} \\ \frac{\partial \Lambda}{\partial \varphi^* \partial \psi^*} & \frac{\partial \Lambda}{\partial \theta^* \partial \psi^*} & \frac{\partial \Lambda}{\partial \psi^{*2}} \end{bmatrix}^T, \quad (69)$$

FIGURE 8: The value of Λ when $\varphi^* = -60^\circ$.FIGURE 9: The value of Λ when $\varphi^* = -30^\circ$.

where

$$\frac{\partial \Lambda}{\partial \varphi^{*2}} = -4\Lambda + \frac{15}{4} \sin(\varphi^*) \sin(2\theta^*) \sin(2\psi^*) (1 + 3 \cos(2\varphi^*)),$$

$$\frac{\partial \Lambda}{\partial \theta^{*2}} = -4\Lambda,$$

$$\frac{\partial \Lambda}{\partial \psi^{*2}} = -4\Lambda,$$

$$\begin{aligned} \frac{\partial \Lambda}{\partial \varphi^* \partial \theta^*} &= 4 \sin(2\varphi^*) \sin(2\theta^*) \cos(2\psi^*) \\ &\quad + \frac{1}{2} \cos(\varphi^*) \cos(2\theta^*) \sin(2\psi^*) (7 - 9 \cos(2\varphi^*)), \end{aligned}$$

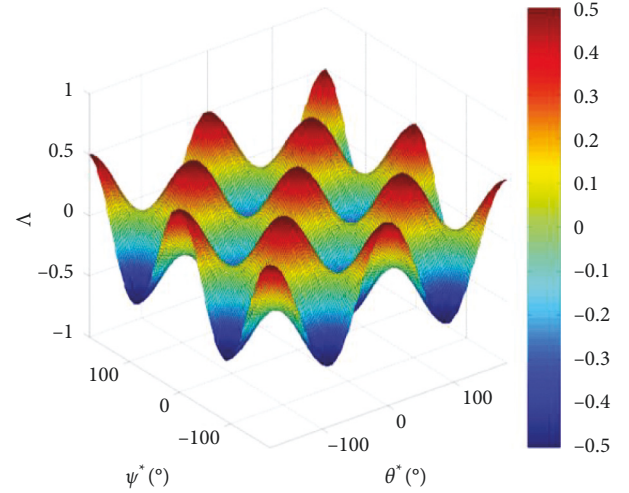
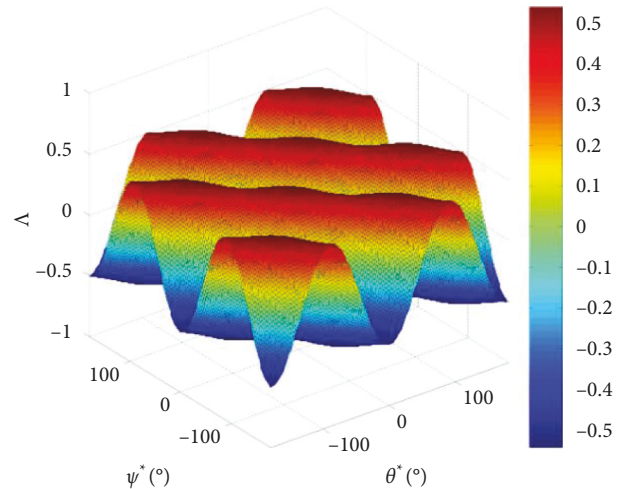
$$\begin{aligned} \frac{\partial \Lambda}{\partial \varphi^* \partial \psi^*} &= 4 \sin(2\varphi^*) \sin(2\theta^*) \cos(2\psi^*) \\ &\quad + \frac{1}{2} \cos(\varphi^*) \cos(2\theta^*) \sin(2\psi^*) (7 - 9 \cos(2\varphi^*)), \end{aligned}$$

$$\begin{aligned} \frac{\partial \Lambda}{\partial \theta^* \partial \psi^*} &= 4 \cos(2\varphi^*) \sin(2\theta^*) \sin(2\psi^*) \\ &\quad + \sin(\varphi^*) \cos(2\theta^*) \cos(2\psi^*) (1 - 3 \cos(2\varphi^*)). \end{aligned} \quad (70)$$

For TEA in the form of the formula (65), there are

$$\frac{\partial \Lambda}{\partial \Theta^*} \Big|_{\text{TEA}} = (0 \ 0 \ 0)^T, \quad (71)$$

$$\frac{\partial \Lambda}{\partial \Theta^{*2}} = \begin{cases} 4(-1)^{n+p} \begin{bmatrix} 1 & 0 & 0 \\ 0 & 1 & 0 \\ 0 & 0 & 1 \end{bmatrix} & m \text{ is even} \\ 4(-1)^{n+p} \begin{bmatrix} (-1)^m & 0 & 0 \\ 0 & (-1)^m & (-1)^{m-1/2} \\ 0 & (-1)^{m-1/2} & (-1)^m \end{bmatrix} & m \text{ is odd.} \end{cases} \quad (72)$$

FIGURE 10: Value of Λ when $\varphi^* = 30^\circ$.FIGURE 11: Value of Λ when $\varphi^* = 60^\circ$.

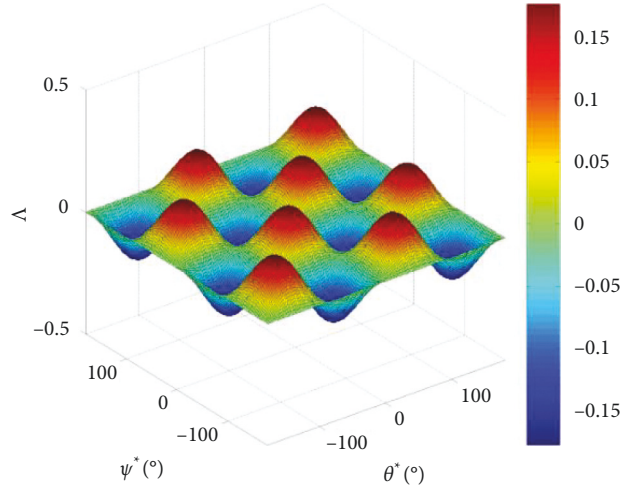
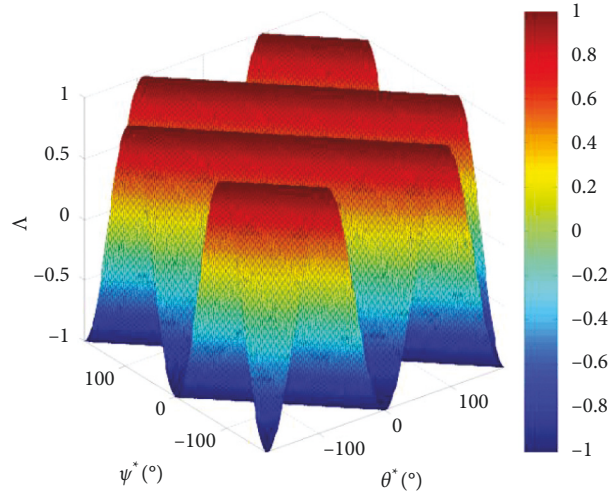
FIGURE 12: Value of Λ when $\varphi^* = 45^\circ$.FIGURE 13: Value of Λ when $\varphi^* = 90^\circ$.

TABLE 1: Configuration transformation cabin and configuration parameters.

		Replenishment vehicle	Replenished vehicle	One line	L configuration
Mass (kg)		22000	22000	44000	44000
	I^x	1.30	1.30	2.60	15.23
	I^y	6.17	6.17	39.56	14.27
	I^z	6.86	6.86	40.94	26.90
Torque of inertia (10^5 kgm^2)	I^{xy}	0	0	0	6.934
	I^{xz}	0	0	0	0
	I^{yz}	0	0	0	0

It can be seen that if m is even, the eigenvalues of the second-order Hessian matrix are all $4(-1)^{n+p}$. When $n+p$ is even, TEA is the minimum of Λ . When $n+p$ is odd, TEA is the largest value of Λ . If m is odd, then the eigenvalue of the Hessian matrix is $8(-1)^{n+p}$, $4(-1)^{n+p}$, and 0. When $n+p$ is an even number, $\theta^* = \psi^* \pm (n-p)\pi/2$ ($\varphi^* < 0$) and $\theta^* = -\psi^* \pm (n-p)\pi/2$ ($\varphi^* > 0$) (k is an integer) Λ are both

minima -1 ; when $n+p$ is an odd number, $\theta^* = \psi^* \pm (n-p)\pi/2$ ($\varphi^* < 0$) and $\theta^* = -\psi^* \pm (n-p)\pi/2$ ($\varphi^* > 0$) Λ are both maximum 1.

It can be seen from the above analysis that a TEA is a maximum or a minimum. So, the nonlinear feedback control law given by formula (44) can avoid singular points in principle. But, when the initial attitude is not suitable, the

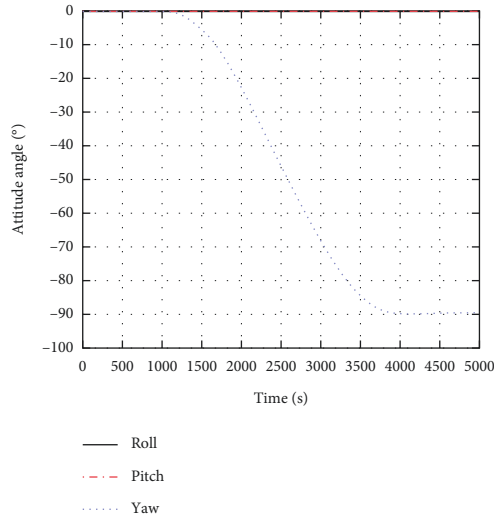


FIGURE 14: Relative attitude angles of replenishment vehicle and replenished vehicle.

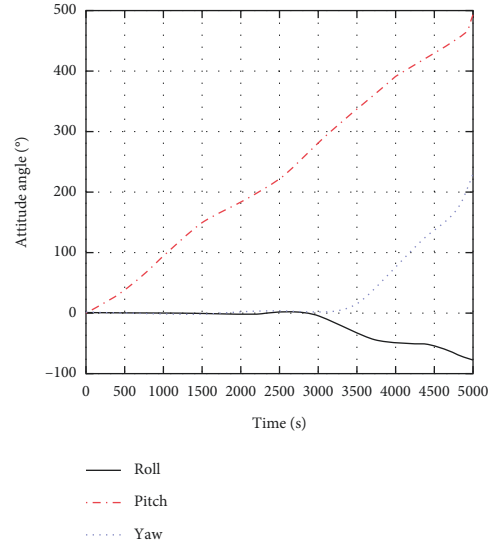


FIGURE 16: Attitude angle of replenishment vehicle in free floating.

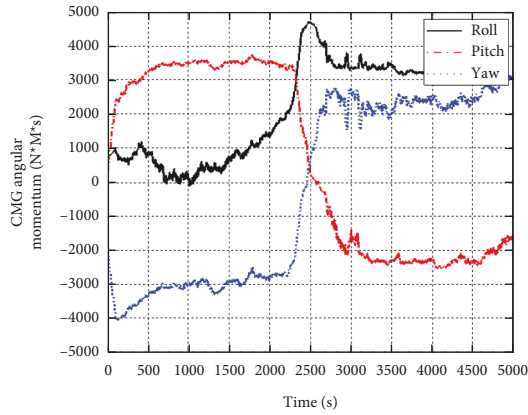


FIGURE 15: Angular torque of CMG under directional stability.

system may still pass through the singular surface during the stabilization process. For example, if the initial angular rate of attitude is relatively large, the system is likely to reach the singular surface before stabilization. Therefore, whether the nonlinear control law can effectively drive the system to TEA is closely related to the initial attitude. If the reference input signal z_d is selected reasonably, the singularity may be avoided in some programs, and the system will approach TEA along the ideal trajectory.

6. Numerical Examples of Configuration Transformation Process

It is assumed that the mass characteristics of the two sections are shown in the table (Table 1).

Suppose that the configuration transformation process takes 5000 seconds, and in the first 1000 seconds, the replenished vehicle is pushed out 5 meters along the longitudinal axis of the replenishment vehicle with a mechanical

arm at a constant speed; when 1000 seconds to 4000 seconds, rotate the replenished vehicle 90° around the negative direction of the yaw axis of the replenishment vehicle. Considering the transfer time and the speed limit of the end of the manipulator, adopt the rotation process of acceleration uniform deceleration. When 1000 seconds to 2000 seconds, rotate the replenished vehicle with constant acceleration, when 2000 seconds to 3000 seconds, rotate with uniform speed, and when 3000 seconds to 4000 seconds, rotate with uniform deceleration. The ideal situation is that when the replenished vehicle rotates 90° relative to the replenishment vehicle, the angular velocity of the relative replenishment vehicle can just be reduced to zero. From 4000 seconds to 5000 seconds, the replenished vehicle is pulled to the lateral interface of the node cabin at a constant speed along the y -axis direction of the replenishment vehicle by the mechanical arm to complete the redocking. From the process of configuration transformation, the relative attitude of the replenishment vehicle and the replenished vehicle is mainly reflected in the yaw axis.

In the simulation model, the replenishment vehicle is a rigid body dynamic model with flexible appendages. The solar panel of the replenished vehicle is retracted during the transfer process, regardless of the influence of its flexible mode, the flexibility of the manipulator, and its dynamic relationship. It is assumed that it can move according to the planned ideal trajectory, and the influence of atmospheric disturbance is considered during the transfer process. In the process of configuration transformation, the replenished vehicle to be transferred is in an uncontrolled state, and the whole system is controlled by a set of CMGs of pentagonal pyramid configuration. The nominal angular torque capacity of each CMG is 1000 nms, and the minimum angular torque on the angular torque envelope of each CMG is 4200 nms. It is still assumed that the combined body runs in a circular orbit 400 km away from the earth's surface, and the orbital angular velocity is lower ω_0 is a constant value of 0.0011 rad/s, and the sampling period is 200 ms. The initial attitude

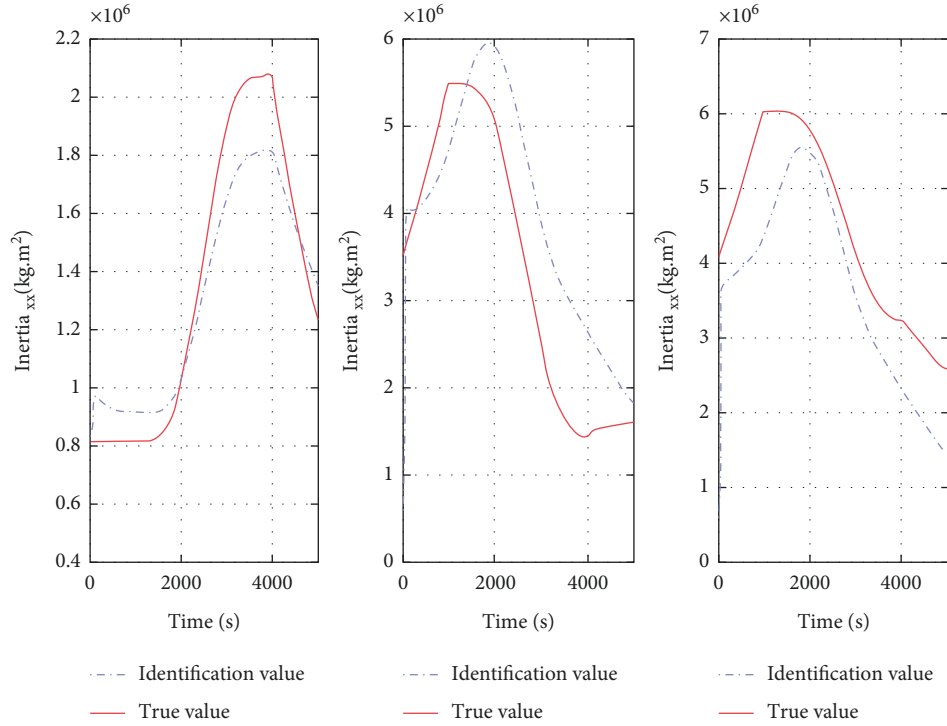


FIGURE 17: Main inertia identification results.

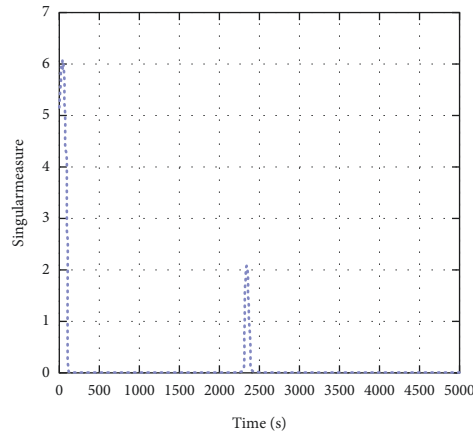


FIGURE 18: CMG singularity measure for earth-oriented stability.

angle and angular velocity are assumed to be $1 \theta = [0.0007 \ 0.0008 \ 0.001]^\circ$, $\dot{\theta} = [0.001-0.001 \ 0.001]^\circ/\text{s}$. The angular torque of the initial CMG is calculated from the initial frame angle of each CMG in the pentagonal pyramid configuration.

Without considering the influence of the manipulator, the relative attitude of the replenishment vehicle and the replenished vehicle in the transfer process is shown in Figure 14. If the replenishment vehicle is in the uncontrolled free-floating state during the configuration transformation, the attitude motion of the replenishment vehicle during the transfer process is shown in Figure 15. If the angular torque management of CMG is not carried out in the process of configuration transformation, and the replenishment vehicle maintains directional stability to the ground, the angular

torque that CMG needs to absorb in the process of configuration transformation is shown in Figure 16. As can be seen from Figure 17, if the replenishment vehicle is not controlled during the transfer process, the attitude angle drift is too large. As shown in Figures 16 and 18, if the replenishment vehicle is strictly oriented to the ground during the transfer process, the disturbance angular torque absorbed by CMG will be large and reach saturation quickly, which will affect the accuracy of the transfer process.

After torque management is adopted, the identification results of the parameter identification unit are shown in Figures 17 and 19 when supplying the narrow TEA of the aircraft attitude tracking system during the transfer process. The closed-loop identification effect of the least square

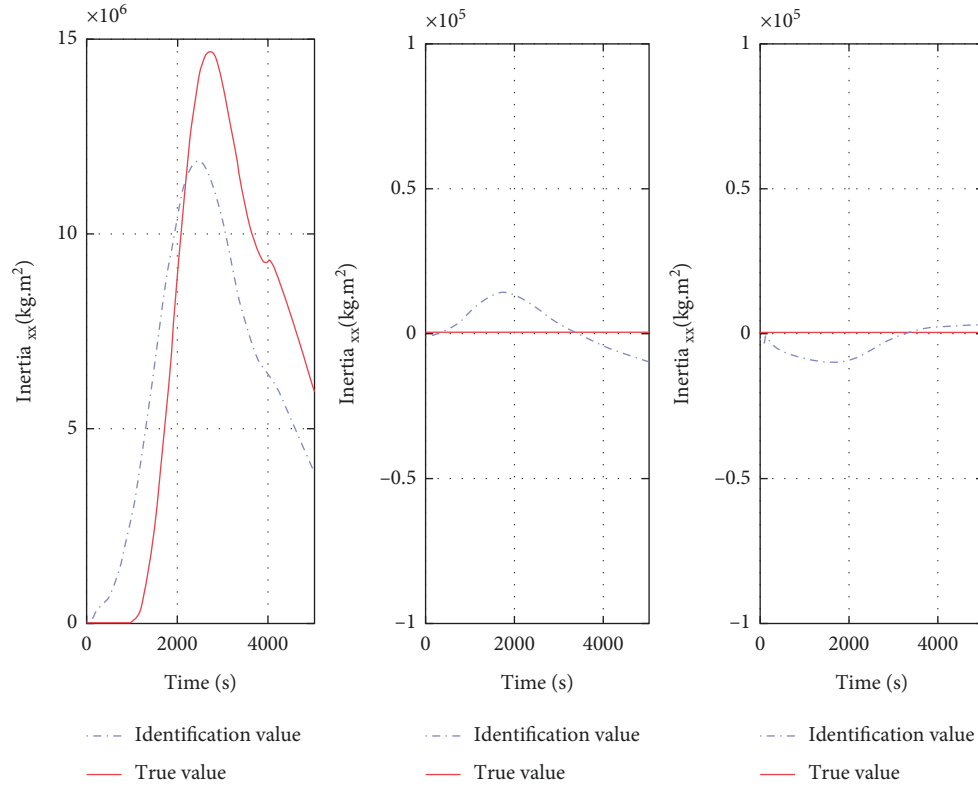


FIGURE 19: Identification result of inertia product.

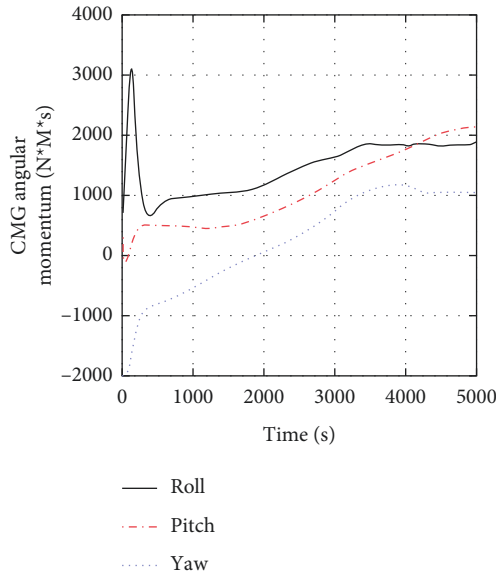


FIGURE 20: CMG angular torque (narrow TEA tracking).

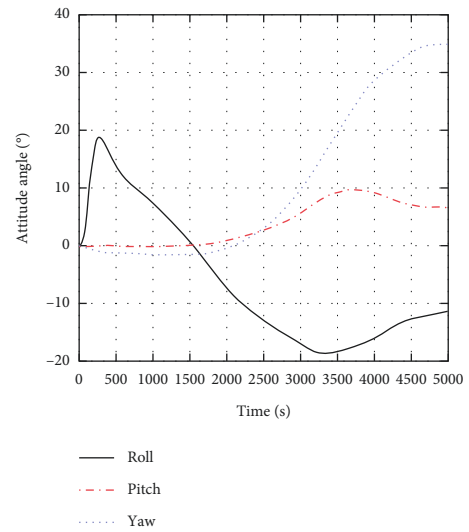


FIGURE 21: Attitude angle of replenishment vehicle.

method with bounded gain forgetting factor is ideal, and it can track the changing torque of inertia of the system in the whole configuration transformation process.

The angular torque and attitude angle stored in CMG are shown in Figures 20–25. After the angular torque planning, the angular torque of CMG is strictly controlled within its capacity range during the whole transfer process (Figures 20

and 22), and the singular measure of CMG is far away from zero (Figure 23). The attitude maneuver of the replenishment vehicle is mainly reflected on the yaw axis (Figures 21 and 24), which can be verified by the relative motion of the replenishment vehicle and the replenished vehicle during the transfer process. In the controller design, the change history of nine states of the equivalent linear system is shown in Figure 25. Except the fifth state needs to track the time-

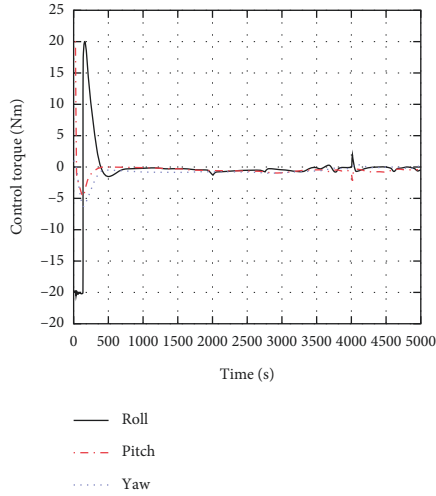


FIGURE 22: Control torque (narrow TEA tracking).

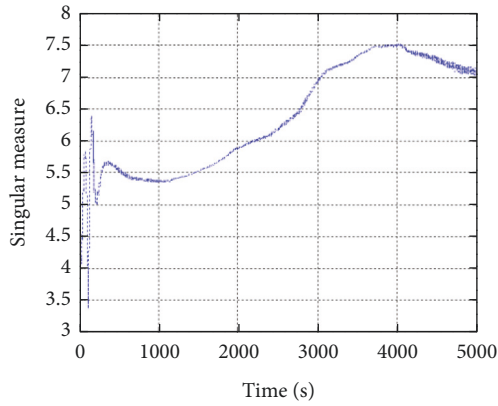


FIGURE 23: CMG singular measure (narrow TEA tracking).

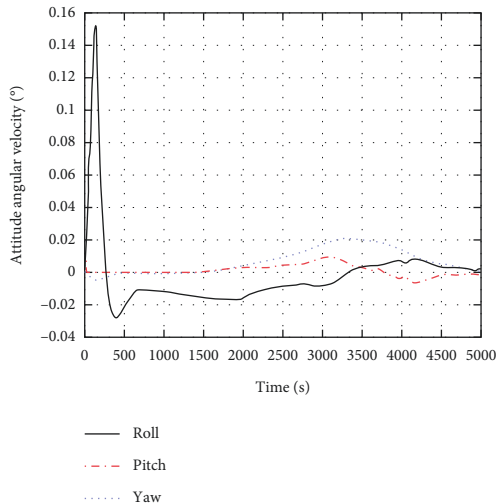


FIGURE 24: Attitude angular velocity of replenishment vehicle.

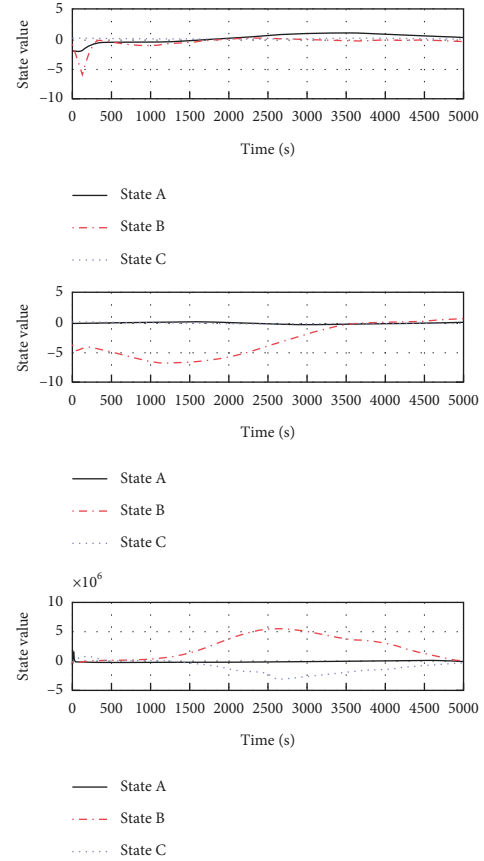


FIGURE 25: Equivalent linear system state variables.

varying reference input and the eighth rolling/pitching inertia product changes constantly during the transfer process, the other amplitudes fluctuate less, and the dynamic effect is ideal.

7. Conclusion

This paper studies the control problem of the variable mass body in the process of on-orbit service. Different from the traditional method, the feedback linearization method of the nonlinear system is used to design the controller. By realizing the tracking of narrow TEA in the process of configuration transformation, the error caused by the angular deviation between narrow TEA and earth orientation attitude caused by the large change of moment of inertia is avoided, and the ACMM controller is obtained. In order to improve the input information accuracy of the ACMM controller, the least square method with a bounded gain forgetting factor is introduced to track the real variable parameters. This method does not need continuous excitation. A joint attitude control/angular momentum management controller is designed to effectively stabilize the system and reduce the angular momentum saturation of the attitude control system during on-orbit service. In the numerical simulation of the configuration transformation process, we compared the changes in CMG angular momentum management in the configuration transformation process. If the supply aircraft is kept strictly oriented to the

ground during the transfer process, the disturbance angular momentum absorbed by CMG will quickly reach saturation and need to be unloaded, which will affect the accuracy of the transfer process. If CMG management is carried out and the least square method with bounded gain forgetting factor is used for closed-loop parameter identification, CMG saturation is effectively controlled. This shows that the ACMM controller can track the changing moment of inertia of the system, which provides a solution to the problem of variable quality control in on-orbit service.

Data Availability

The data used to support the findings of this study are available from the corresponding author upon request.

Conflicts of Interest

The authors declare that they have no conflicts of interest.

References

- [1] B. Wu, X. Cao, and Z. Li, "Multi-objective output-feedback control for microsatellite attitude control: an LMI approach," *Acta Astronautica*, vol. 64, no. 11-12, pp. 1021-1031, 2009.
- [2] Z. Chu, Y. Lei, and D. Li, "Dynamics and robust adaptive control of a deployable boom for a space probe," *Acta Astronautica*, vol. 97, pp. 138-150, 2014.
- [3] G.-S. Huang and H. J. Uang, "Robust adaptive pid tracking control design for uncertain spacecraft systems: a fuzzy approach," *IEEE Transactions on Aerospace and Electronic Systems*, vol. 42, no. 4, pp. 1506-1514, 2006.
- [4] J. Qin, *Robust Control for Uncertain Linear Singularly Perturbed Systems [D]*, School of information, Zhejiang University, Hangzhou, 2007.
- [5] Y. Zhou and J. Zeng, "Nonlinear robust H_∞ control method for spacecraft attitude maneuver," *Control and Decision*, vol. 32, no. 4, pp. 625-631, 2017.
- [6] G. Yuan, X. Shi, and Li long, "Design of adaptive robust attitude controller for spacecraft," *Systems engineering and electronic technology*, vol. 34, no. 12, pp. 2524-2528, 2012.
- [7] X. Tong and D. Li, "Attitude static output feedback of Spacecraft Based on iterative LMI [J]," *Acta Astronautica Sinica*, vol. 28, no. 3, pp. 539-544, 2007.
- [8] X. Yang, H. Gao, and P. Shi, "Robust orbital transfer for low earth orbit spacecraft with small-thrust," *Journal of the Franklin Institute*, vol. 347, no. 10, pp. 1863-1887, 2010.
- [9] J. Liang, S. Xiao-hong, Y. Zhao, Y. Cai, and H. Zhang, "Attitude maneuvering method of agile satellite based on variable structure controller," *Navigation and Control*, vol. 19, no. 2, 2020.
- [10] Y. Lei, L. Liu, Y. Cui, Z. Yue, and J. Kang, "A time-varying structure modal parameter estimation method in deterministic evolution for launch vehicle," *Journal of Astronautics*, vol. 41, no. 4, 2020.
- [11] V. D. Kharlat, "Linear theory of creep for a growing body," *Proc Leiaingroll*, vol. 49, p. 93, 1966.
- [12] M. Rognant, C. Cumer, and J.-M. Biannic, "Autonomous assembly of large structures in space: a technology review," in *Proceedings of the 8th European Conference for Aeronautics and Aerospace Sciences (EUCASS)*, Springer, Madrid, Spain, 1 July 2019.
- [13] C. Hu, L. Cao, L. Zhao, and Na Wang, "Model predictive control-based steering control of unmanned ground vehicle with tire blowout," *Journal of Tianjin University*, vol. 52, no. 5, 2019.
- [14] S. Wang and X. Cao, "On-line mass-Property identification algorithm research for satellite," in *Proceedings of the 2006 Chinese Control Conference*, IEEE, Harbin, China, 7 August 2006.
- [15] W. Edward, L. Chris, and W. M. Robert, "On-line guro-based mass-property identification for thruster controlled spacecraft using recursive least squares," in *Proceedings Of the 45th IEEE International Midwest Symposium on Circuits and System*, pp. 1-8, IEEE, Tulsa, OK, USA, 4 August 2002.
- [16] H. Liu, Q. Zhang, and Y. Guo, "Online identification of morphing aircraft model parameters based on recursive least square method," *Air & Space Defense*, vol. 3, no. 3, pp. 103-110, 2020.
- [17] N. Arutyunyan, "Boundary value problem in the theory of creep for a body with accretion," *Journal of Applied Mathematics and Mechanics*, vol. 41, 1977.
- [18] G. Sun, J. Xie, and J. Wang, "Ship course identification model based on recursive least squares algorithm with dynamic forgetting factor," *Journal of Computer Applications*, vol. 38, no. 3, 2018.